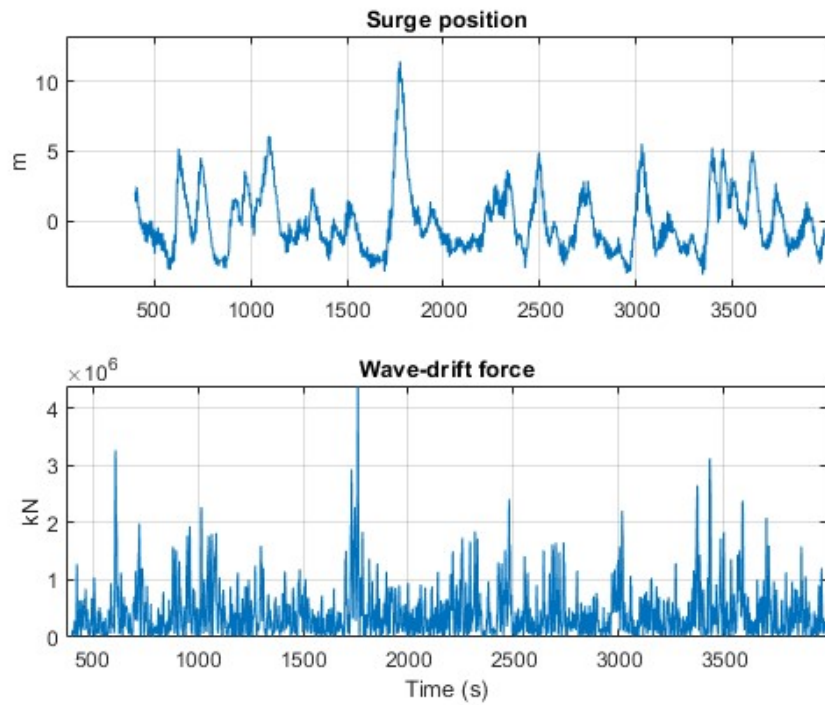




SINTEF



Project Report

Possibility of loss of position for dynamically positioned semi-submersibles due to impulsive wave load

Authors:

Karl Erik Kaasen, Halgeir Ludvigsen

Report No: OC2021 F-079

Client :

Petroleum Safety Authority Norway

Project Report

Possibility of loss of position for dynamically positioned semi-submersibles due to impulsive wave load

KEYWORDS:Marine Technology
Hydrodynamics
Semi-Submersible
Dynamic Positioning
Vessel
Motion
Response
Impulse
Wave drift
Morison
Kalman Filter
Probability
Delay**VERSION**

1

DATE

2021-09-30

AUTHORS

Karl Erik Kaasen, Halgeir Ludvigsen

CLIENT(S)

Petroleum Safety Authority Norway

CLIENT'S REFERENCE

Lars Geir Bjørheim

PROJECT NO.

302006215

NO. OF**PAGES/APPENDICES:**

47/0

SUMMARY**Abstract heading**

Incidents of loss of position for dynamically positioned semi-submersibles in moderate sea states have led to the hypothesis that the cause could be a large slamming load from a tall and steep wave. A study is carried out to check the hypothesis. Analysis of the characteristics of a semi with DP shows that due to the wave + noise filter in the DP controller, a sudden disturbance is not counteracted effectively by the DP system. Still, a slamming load will not cause a large position deviation. The likely cause of excessive excursion is found to be wave-drift load from a group of tall and short waves. For a semi-submersible, wave-drift loads can be strongly amplified as a result of viscous forces on the columns, as shown by applying the Exwave formula. For the analysis, a simplified model of a DP-controlled vessel has been developed. Further, vessel motion has been simulated with Simo for five sea states of short period, and probabilities of exceedance of given limits have been estimated.

PREPARED BY

Karl E. Kaasen

**CHECKED BY**

Halvor Lie

APPROVED BY

Henning Braaten

REPORT NO

OC2021 F-079

ISBN**CLASSIFICATION**

Restricted

CLASSIFICATION THIS PAGE

Restricted

Document history

VERSION	DATE	VERSION DESCRIPTION
1.0	2021-09-30	First Version

Table of contents

1	INTRODUCTION	5
2	PRINCIPLE OF DYNAMIC POSITIONING	5
3	LOADING MECHANISMS	6
3.1	Slamming load.....	6
3.2	Wave frequency viscous load	10
3.3	Wave-drift load	12
4	EFFECT OF CURRENT AND WAVE CONDITION ON WAVE DRIFT	14
5	RESPONSE CHARACTERISTICS OF DYNAMICALLY POSITIONED VESSEL	15
5.1	Model.....	15
5.2	Example.....	18
5.2.1	Model data	18
5.2.2	Filter characteristics	19
5.2.3	Response of dynamically positioned vessel	20
5.2.3.1	Response with and without thruster delay	20
5.2.3.2	Analysis of impulse response.....	22
5.2.3.3	Importance of the initial state	26
6	SIMULATION OF MOTION IN IRREGULAR SEA	27
6.1	SIMO model	27
6.2	Sea states	29
6.3	Simulations.....	31
6.3.1	Parameter variation.....	31
6.3.2	Simulation results	33
6.3.2.1	Deepsea Bergen.....	33
6.3.2.2	The Exwave semi	34
6.3.2.3	Comparison of results fro the two semi-submersibles.....	35
6.3.3	Probability of loss of position	36
6.3.4	Dependence of response on spectral peak period - probability curves.....	39
6.3.5	Further analysis of results	40
7	THE INFLUENCE OF THE DP SYSTEM ON THE RESPONSE	43
8	SUGGESTIONS FOR FURTHER WORK	44
9	ACKNOWLEDGEMENT	44
10	CONCLUSION	44



11 REFERENCES 46

1 INTRODUCTION

According to Petroleumstilsynet (The Petroleum Safety Authority of Norway) there have been a number of cases when large wave forces - yet under normal operating conditions - have caused loss of position for DP-controlled semi-submersibles, cf. [1], [2]

One hypothesis has been that the platform's excursion was caused by slamming from a high and steep single wave created by statistical coincidence. Such a load could well be regarded as one that causes the same effect as that of an ideal impulse load – i.e., a load of infinite magnitude, but with infinitesimal duration, such that the time-integrated product of magnitude and duration becomes finite and non-zero.

When an impulse hits a mechanical body that is free to move, it will cause a step change in the body's velocity and kinetic energy. In practice, a load can be regarded as approximately impulsive, provided the body's velocity is not affected noticeably by reaction forces during the time the force is acting. For a moored or dynamically positioned vessel, the reaction forces are restoring forces and damping forces.

Another possible cause of loss of position in seas of moderate height could be large viscous force ("Morison load" [5], [6]) on the semi's columns from a not so steep, but tall wave. In contrast to models based on potential theory, the Morison equation has an additional viscous term. Compared to a slamming load, the wave force on a column would be smaller, but its duration longer, which might have an identical effect on the semi's response

A third effect could be that of extreme wavedrift (i.e., extreme for the wave height), i.e., the slowly varying force caused by non-linear forcing mechanism in irregular seas. In this case, a group of tall and steep waves could in its passing create a significant force of less than a minute's duration. The load would in this case not qualify as an approximate impulse load, but still happen quickly enough to escape the full restoring action of the DP system.

These three types of loads will be treated further in Chapter 3.

2 PRINCIPLE OF DYNAMIC POSITIONING

The response of the DP system to the wave disturbance will be less immediate as that of mooring system. This is because the thrusters need some time to react to the changing demand for force from the controller, and because the filter for reduction of wave frequency motion and measurement noise will add a delay.

The detailed functioning of a DP controller is the secret of the manufacturer. Still, it is expected that any system will perform Proportional + Integral + Derivative (PID) control in combination with model-based filtering. A basic schematic of a DP system is shown in Figure 2-1. The purpose of the filter is to remove the wave-frequency (WF) component from the measured position to leave the low frequency (LF) component of motion. The reason for this is that the WF loads are so forceful they cannot be counteracted by the thrusters. Letting the WF part of the position error through to the thruster system via the feedback would result in futile WF thrust action that would only create wear on the thrusters and unpleasant audio noise for the crew. In addition to reducing the amount of WF in the feedback loop, the filter also filters off measurement noise.

Like a mooring system, a DP system can be regarded as a spring plus damper system, with the difference that the spring and damping actions are created synthetically. As described above, another difference is the delay of reaction from the DP system. The integral action of the DP ensures zero stationary (mean) error, a

property that the mooring system lacks, unless the mooring lasses are run continuously. One great advantage with DP over mooring is that a large damping level – e.g., 70 % of critical – can be set.

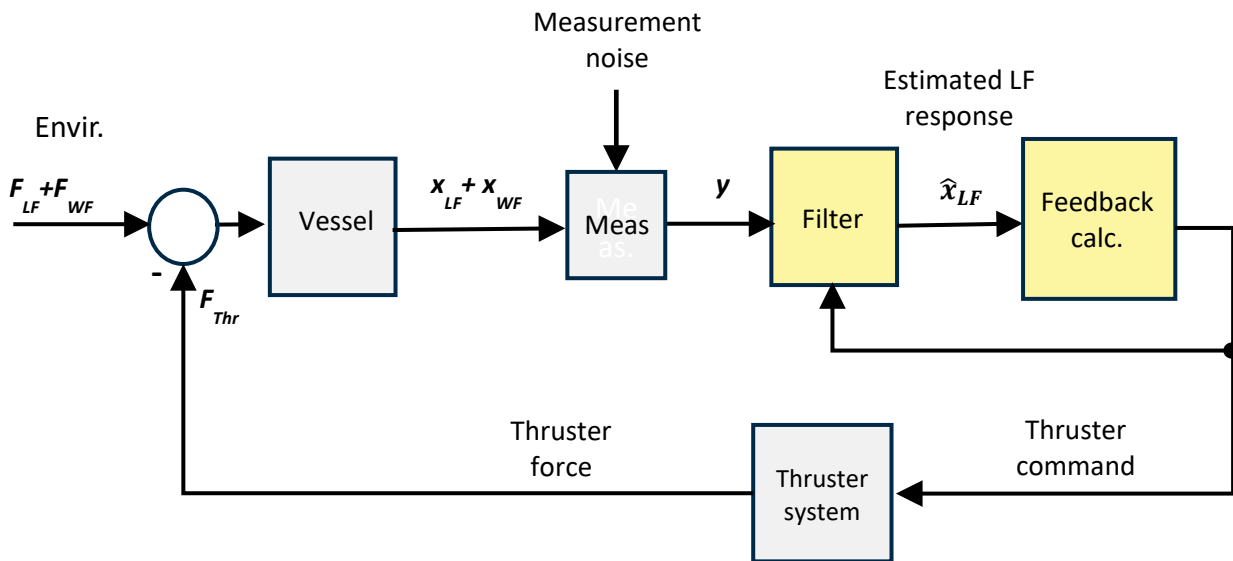


Figure 2-1 Simplified block diagram of a typical DP system. The yellow boxes constitute the DP controller.

3 LOADING MECHANISMS

As proposed in the introduction, three different "mechanisms" can be thought to create sudden loss of position:

1. Slamming load from a steep single wave
2. Viscous load from tall single wave
3. Wavedrift load from a group of large waves

In the following these will be treated briefly.

3.1 Slamming load

It may happen that a steep and tall wave will rise and break in the immediate front of a column and create damaging water pressure where it hits. In the modelling world, this is seen as a coincidental combination of the phase angles in the components that constitute the irregular sea. Such slamming has very short duration and can well be regarded as coming close to the notion of impulse load. When a large area of the column's side is hit, the total slamming force could be so large as to drive the vessel off position.

The linear spring-mass-damper system is frequently used as a simplified model in analysis of mechanical dynamic systems, such as moored or dynamically positioned vessels. The system is modelled by the simple differential equation:

$$m\ddot{x} + c\dot{x} + kx = F \quad (1)$$

where x is the position, \dot{x} the velocity, \ddot{x} the acceleration, and F the driving force. The parameters m , c and k are the coefficients of mass, damping and stiffness, respectively.

For a spring-mass-damper system initially at rest, the position response to an ideal impulse load, $F = I$, becomes

$$x(t) = \frac{I}{m\beta} \exp(-\alpha t) \sin \beta t \quad (2)$$

(provided the damping is not greater than critical). The response is seen to consist of a sinusoidal oscillation which is damped by a declining exponential function. Denoting the coefficients of mass, damping and stiffness by m , c and k , respectively, the decay exponent (α) and the natural frequency (β) become:

$$\alpha = \frac{c}{2m}$$

$$\beta = \sqrt{\frac{k}{m} - \left(\frac{c}{2m}\right)^2} \quad (3)$$

The excursion reaches its maximum value at the time $t_{max} = \tan^{-1} \frac{\beta}{\alpha}$. The maximum becomes:

$$x_{max} = x(t_{max}) = \frac{I}{\sqrt{mk}} \exp\left(-\frac{\alpha}{\beta} \tan^{-1}\left(\frac{\beta}{\alpha}\right)\right) \quad (4)$$

Introducing the damping ratio, $\zeta = \alpha/\sqrt{\alpha^2 + \beta^2}$, x_{max} can be formulated as

$$x_{max} = \frac{I}{\sqrt{mk}} \exp\left(-\frac{\zeta}{\sqrt{1-\zeta^2}} \tan^{-1}\left(\frac{\sqrt{1-\zeta^2}}{\zeta}\right)\right) \quad (5)$$

When the damping is zero ($c = 0 \rightarrow \zeta = 0$), the maximum excursion becomes I/\sqrt{mk} . When the damping is increased, the maximum excursion is reduced. This is shown in Figure 3-1. For a damping ratio of $\zeta = 0.1$ (10%), which may represent the surge damping of a moored vessel, the peak of the excursion is 0.86 times that of the non-damped vessel. For a damping ratio of 0.7, which is typical for a DP system, the maximum response is reduced to 0.46. Figure 3-2 shows the impulse responses for the three values of damping ratio.

It is noted from Eq. (5) that, provided the damping ratio remains constant, the maximum offset is inversely proportional to the square root of the stiffness, k . This means that if one wants to reduce the maximum value of the response by a factor of two, the stiffness of the mooring system or DP system (i.e. the proportional gain) must be quadrupled.

As explained above, although the damping value of $\zeta = 0.7$ is characteristic for a DP system, the impulse response of a real DP system must be expected to be greater than shown in the figures due to the delay of the filter and the thruster dynamics. This is treated further in Chapter 5.

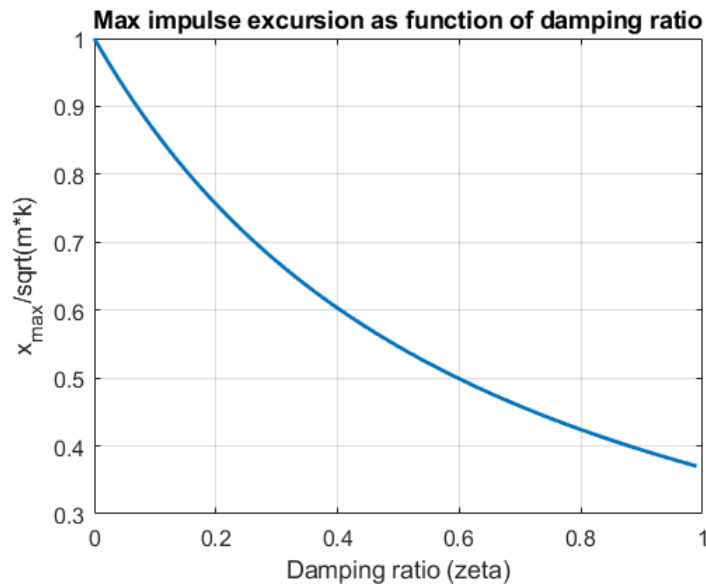


Figure 3-1 Dependence of max impulse response on damping ratio. The curve is normalized by the max response of the non-damped system ($c = 0 \rightarrow \zeta = 0$)

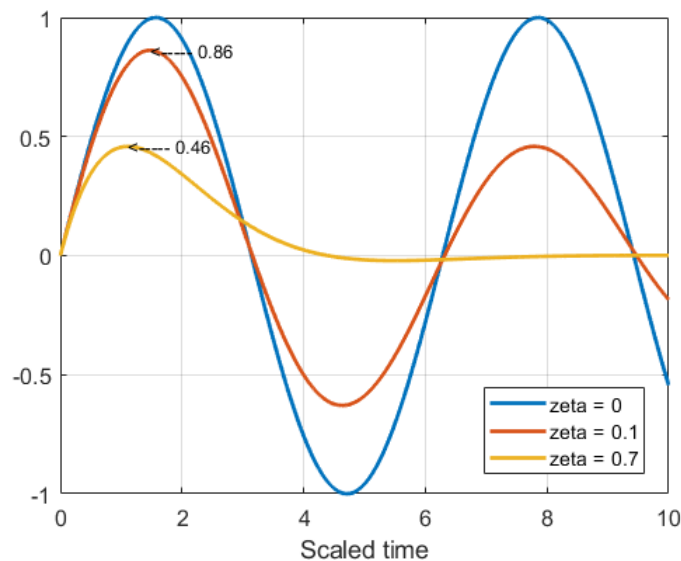


Figure 3-2 Impulse responses of mass-damper-spring system for different values of damping ratio, ζ .

Neglecting for the moment the delay in the response due to delays in filter and thruster response, we try to find an impulse load that is capable of driving a vessel substantially away from the mean position. The vessel is taken to be the size of Deepsea Bergen, which has a total mass of 29 945 metric tonnes, including hydrodynamic added mass at zero frequency. The stiffness of the DP system is assumed such that the undamped natural period becomes 100 seconds, which gives a stiffness of $k = 120 \text{ kN/m}$. The damping ratio is assumed to be $\zeta = 0.7$, including the hydrodynamic damping. The "substantial" excursion is taken as 7 m (which is inspired by the event reported in [1] and [2]). Using this value for x_{max} in Eq. (5), the impulse becomes:

$$I_1 = 29\,000 \text{ kNs} \tag{6}$$

We will compare this value with the result from a slamming model: We consider a slamming event in a sea state of 7 m significant height (H_s) and a spectral peak period (T_p) of 9.1 s. This is a state of steep waves but it may well be within the limit of most offshore operations (It is identical to the middle case in Table 6-3, or "base case" considered below).

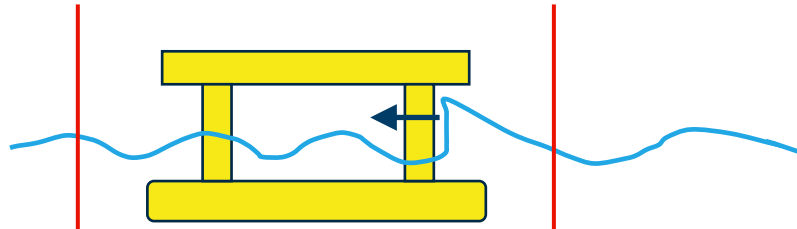


Figure 3-3 Sketch of slamming event. The red lines show the position limits for the vessel. If the vessel's centre is driven past any of the lines, this is defined as loss of position.

It is assumed that a vertical "wall" of moving water is formed immediately in front of the semi-submersible's column, cf. Figure 3-3.

The maximum slamming force can be expressed as (cf. [4]):

$$F = 2\pi\rho hRV^2 \quad (7)$$

Here, ρ is the density of water, h the height of the slamming area, i.e., the height of the column surface hit by the wave, R the radius of the column and V the horizontal speed of the water.

Some further assumptions are made:

The height h of the slamming area is taken as the most probable highest wave amplitude in three hours' time. The formula for the most probable maximum, assuming Rayleigh-distributed peaks is:

$$h = \sigma\sqrt{2 \log(N)} \quad (8)$$

Here, $\sigma = H_s/4$ is the standard deviation of the wave, and N is the number of zero up-crossings, Assuming the mean zero up-crossing period to be $T_z = T_p/1.2 = 7.6$ s, the average number of peaks in 3 hours is $N = 1421$. (The ratio between T_z and T_p depends on the shape of the sea spectrum, cf. [3]. The value 1.2 corresponds to a narrow-banded Jonswap spectrum with the parameter γ equal to 5).

From the above, the most probable maximum in three hours becomes:

$$h = 6.7 \text{ m}$$

The radius of the front columns of Deepsea Bergen is $R = 4.5$ m. The wave speed (celerity) is calculated from (assuming deep water), cf. [4]:

$$V = \frac{gT_p}{2\pi} \quad (9)$$

where g is the gravitational acceleration. The speed becomes:

$$V = 14.2 \text{ m/s}$$

Inserting these parameter values in Eq. (7) gives for the initial slamming force on the column:

$$F = 39\,000 \text{ kN}$$

This is the force that arises in the instant when the "wall of water" hits the column. According to [4] the duration of the slamming event can be estimated by the formula

$$T = \frac{13R}{32V} \quad (10)$$

which gives $T = 0.129$ s. However, in this time the force will decline towards zero. To estimate the impulse load, it is reasonable to assume an effective duration of $T_e = T/2 = 0.064$ s. The impulse then becomes $I = T_e \cdot F = 2\,500$ kNs.

If the wave hits the front of the semi in such a way that the slamming conditions are fulfilled for each of the two front columns, the impulse load will be doubled, and we get:

$$I_2 = 5\,000 \text{ kNs} \quad (11)$$

This value is significantly lower than the impulse I_1 in Eq. (6), which is the impulse capable of moving the vessel 7 m out of the mean position from a state of rest. For comparison, the slamming impulse I_2 will move the vessel 1.2 m.

It is pointed out that the calculation of the slamming load is rather crude and rests on a number of assumptions. However, these assumptions are made such that the impulse load I_2 becomes a worst-case event for the given significant wave height of 7 m. Other parameter combinations could be tried. Changing the wave parameters and the duration of the time period under consideration will not give drastic change.

In the above calculation it is assumed that the column has circular cross-section. For a square column and when the wave hits a side perpendicularly, it must be assumed that the peak load will be greater and the duration of the load shorter. When the wave hits diagonally the opposite will happen. In either case, the force-times-duration magnitude of the impulse may not deviate substantially from the estimate for the circular cross section above.

3.2 Wave frequency viscous load

The Morison equation is a heuristic formula for the force on a slender vertical pile extending from the sea-floor from viscous flow, [5] [6].

$$F = \int_{-d}^{\eta} \rho C_M \pi \left(\frac{D}{2}\right)^2 \dot{u}(z) dz + \int_{-d}^{\eta} \frac{1}{2} \rho C_D D |u(z)| u(z) dz \quad (12)$$

Here, $u(z)$ is the depth-dependent speed of water normal to the column's surface, ρ the water density and D the diameter of the column. The integrals are evaluated from the location $(-d)$ on the seafloor and the sea surface. C_M and C_D are the dimensionless coefficients of inertia and drag. These coefficients depend on the Reynolds number and the Keulegan-Carpenter (KC) number [7]. While the value for C_M in most cases will lie around 2, the dependence is stronger for C_D , which also depends on the surface roughness. For Eq. (12) to hold, the pile must be slender, which is loosely formulated as the condition that the diameter must be much smaller than the wavelength. For Deepsea Bergen, the diameter of the columns is less than 1/14'th of the wavelength corresponding to a period of 9.1 s. This must indicate that the Morison formula will apply.

It is only the second integral in (12) that is of interest in the present context. The first integral represents inertia force, which is already included in the potential-flow model for the 1st-order transfer functions (yet with a moderate error due to the linear extension of the model to the non-infinitesimal surface elevation and vessel motion).

The second integral represents viscous loading, which is absent in the potential model. In regular seas of small amplitude, the viscous force will be cyclic and approximately symmetrical about zero. Thus, the force will contribute to the wave-frequency motion of the vessel. When the amplitude is larger the Morison drag (second term in Eq. (12)) becomes more asymmetric, as the positive peaks of force will be larger than the negative peaks. Here, a positive peak of force is taken to correspond to the situation when a wave crest is passing the column. A measure of the force is estimated as follows:

Using a wave of 7 m significant height and $T_p = 9.1$ s as in the example above, the 3-hour most probable maximum wave peak is 6.7 m, as calculated above. Assuming now a sinusoidal wave with this amplitude, the second integral in (12) is evaluated from the bottom of the column at 9.5 m below the SWL (d in Eq. (8)) and up to an height above the still water level (SWL) equal to the wave amplitude of 6.7 m (η in Eq. (8)). Below the SWL the velocity profile declines exponentially as $\exp(kz)$, where k is the wave number and z the vertical distance below the SWL (where z is negative). The value $C_D = 1.0$ was used in the calculation. See [6] for background theory.

The Deepsea Bergen (Figure 6-1) has eight columns. The four columns at the corners have a diameter of 9 m. The peak force on one of these columns resulting from a wave of 6.7 m amplitude becomes 1060 kN. The four columns between the corners have a diameter of 7.4 m and experience a force of 870 kN each. Assuming as a worst case that the force on each column is unaffected by the presence of the others, and that the forces happen simultaneously, we get as an upper bound for the viscous force:

$$F_{visc} = 7\,700 \text{ kN}$$

From the motion characteristics of Deepsea Bergen in the SIMO model (see Section 6.1) we get the corresponding *potential* force for the same wave period: 20 000 kN. The motion amplitude obtained from the SIMO model for a wave amplitude of 6.7 m is 1.44 m. This means that by adding the viscous force to the potential force, we will expect an increase in the motion amplitude of about 40 %, i.e., from 1.44 m to 2.0 m as the 3-hour extreme amplitude in the chosen sea state ($H_s = 7$ m, $T_p = 9.1$ s). This calculation holds if the potential force and the viscous force are in phase. If ninety degrees phase difference is assumed, the increase is only 7 %.

It is reminded that this estimate of F_{visc} is an upper bound, assuming synchronous force on the columns. In addition, viscous *damping* is not taken into the account. It is possible that this damping may outweigh the additional viscous excitation such that the net viscous contribution will be negative.

The conclusion, therefore, is that viscous WF effects will not be a major cause of loss of position.

It is further added that in irregular seas the quadratic nature of the viscous drag in (12) and the asymmetry of the force will cause nonlinear frequency mixing, which will generate components of force outside the WF band, in particular LF components of force. For a wave of amplitude 6.7 m the viscous force corresponding to a wave *trough* is -125 kN on a corner column. This shows the degree of asymmetry of the viscous force. The viscous LF components will be small in comparison with the viscous WF force, but due to their longer persistence they may cause a noticeable increase in the motion. However, this phenomenon belongs to the category of wave drift, which is treated next.

3.3 Wave-drift load

A vessel in regular seas will in addition to the oscillating wave load experience a constant force, the wavedrift force. This force is the result of a nonlinear hydrodynamic forcing mechanism. Based on the methods from potential theory the constant force can be modelled by so-called wave-drift coefficients, which vary with frequency. For a regular wave, the wave drift force will be proportional to the square of the wave amplitude. In irregular seas the wave-drift force will vary slowly about a mean value given by

$$\bar{F} = \int_0^{\infty} C_{WD}(\omega)S(\omega)d\omega \quad (13)$$

Here, $C_{WD}(\omega)$ is the wave-drift coefficient and $S(\omega)$ the wave spectrum. Figure 3-4 shows the wave drift coefficient for surge for Deepsea Bergen. On the whole, a wave-drift coefficient will increase with frequency. The function in the figure will give almost no wave drift for frequencies below 0,5 rad/s – which corresponds to a period of about 13 seconds. Up to 1 rad/s the value of the coefficient has a moderate trend, then it increases dramatically. The tall peak lies between frequencies corresponding to periods in the range 4.5 - 6 seconds. The general increase of the wavedrift coefficient with frequency implies that for spectral seas the mean force will be greater for steep waves, i.e., when the wave spectrum is located to the right on the frequency axes.

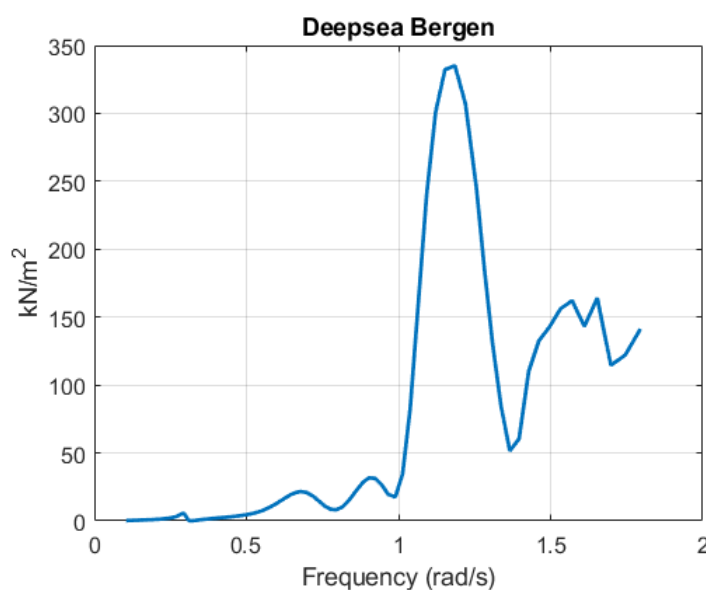


Figure 3-4 Wave drift coefficient of surge

To calculate the slowly varying force the quadratic transfer function (QTF) is needed. The QTF is a function on a two-dimensional frequency domain and is little used. This is because the much simpler Newman approximation [6] usually is found adequate, in particular for semis.

Compared with the linear (1st-order) wave force, the wave drift force in irregular seas will vary slowly (and is therefore frequently referred to as low frequency (LF) wave force). The variation in magnitude can be large. Figure 3-5 demonstrates this. The figure shows surface elevation and wave drift force reconstructed from measurements on a moored semi that had suffered a line breakage in a one-year storm. The large force arising in the middle of the figure was estimated as the cause of the damage. This force, in turn, was caused by a group of high waves, as seen (The difference in the mean force level before and after the large peak is only apparent and due to uncertainty in the calculation). It is characteristic of the wave drift load that it does not change sign, although the wave oscillates about the SWL.

The load in the figure has a duration of about 100 seconds and cannot be said to be an impulse, even approximately (since the positioning system will begin to react well before the termination of the load peak. Still, it is informative that its impulse value, estimated as the area under the curve across the interval between 3 200 s and 3 300 s is in the order of 250 000 kNs. This is vastly more than the values I_1 and I_2 above, cf. Eqs. (6) and (11). It must be noted that the event in the figure concerns a bigger semi-submersible than the Deepsea Bergen and a more severe wave condition than in the calculations above. Still, there is reason to believe that the reported cases of loss of position have been caused by large wave drift force.

Assuming wave drift loading to be the predominant cause of loss of position, the processes of loading and response will be studied further below.

Like the mean wave drift force, also the low frequency variation of force will be greater for steep sea states.

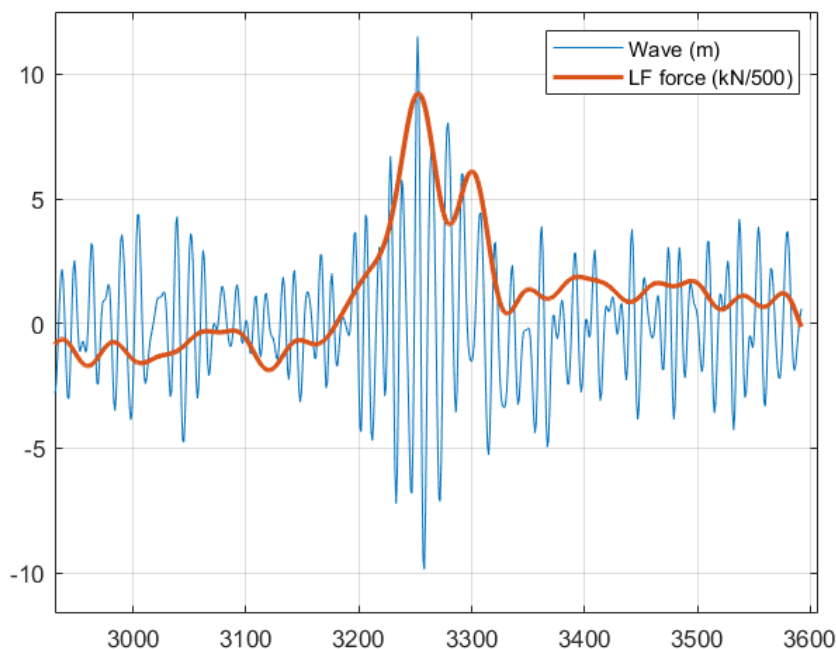


Figure 3-5 Surface elevation and wave drift force in surge. Horizontal axis shows time in seconds (The tallest wave in the figure has a steepness of 0.045, which is about one third of the breaking limit)

4 EFFECT OF CURRENT AND WAVE CONDITION ON WAVE DRIFT

Wave drift coefficients are calculated by methods based on potential theory, i.e., the assumption of inviscid fluid flow. For semi-submersible vessels there may be viscous effects that increase the load significantly. Further, most calculation codes do not take the effect of current into account. The presence of current will change the ratio between the frequency of encounter and the wavelength and cause a change in the wave drift.

One goal of the Exwave joint industry project [8] was to find a way to modify the wavedrift model such that the effects of current and viscosity could be included. To this end a series of laboratory tests were carried out in the Ocean basin at SINTEF Ocean. Two scale models of semisubmersibles were tested. One model represented the Deepsea Bergen (Figure 6-1). The other was an "anonymous" vessel design referred to as the *Exwave semi* (Figure 6-2).

The so-called "Exwave Formula" for correction of wave-drift coefficients reads:

$$C_{WD}(\omega, U_c, H_s) = (1 + C_p U_c \cos \beta_{wc}) C_{WD}^{(pot)}(\omega) + B(\omega)(G U_c \cos \beta_{wc} + H_s) \begin{pmatrix} \cos \beta \\ \sin \beta \end{pmatrix} \quad (14)$$

where

ω	= Wave frequency (rad/s)
U_c	= Current speed (m/s)
H_s	= Significant wave height (m)
$C_{WD}(\omega, U_c, H_s)$	= Corrected wave drift coefficient (N/m^2)
C_p	= Potential flow wave-current interaction coefficient (s/m) ($C_p = 0.25$ s/m is a typical value)
β_{wc}	= Angle between wave direction and current direction
$C_{WD}^{(pot)}(\omega)$	= Original un-corrected wave drift coefficient from potential theory (N/m^2)
$B(\omega)$	= Correction factor depending on geometry of semisubmersible (N/m^3)
G	= Viscous wave-current interaction coefficient (= 10 s)
β	= Wave direction relative to vessel x axis.

The formula consists of two parts. The first is a correction for the effect of current on the potential-flow wave drift coefficient. The second part is a correction for viscous correction when current exists plus a correction for wave height dependence. Eq. (14) applies to surge (x) and sway (y). The meaning of the last parenthesis is that $\cos \beta$ is to be used for x and $\sin \beta$ for y.

Various versions of the formula exist, differing in how the coefficient $B(\omega)$ is calculated. This coefficient depends in particular on the number and sizes of columns. In the present study, $B(\omega)$ is calculated according to [14]. A somewhat different formula is presented in [9].

Figure 4-1 shows an example of the result of applying of the correction formula. The wave drift coefficient is the same as is shown in Figure 3-4. It is seen that the correction has a substantial effect, in particular in the frequency range below 1 rad/s.

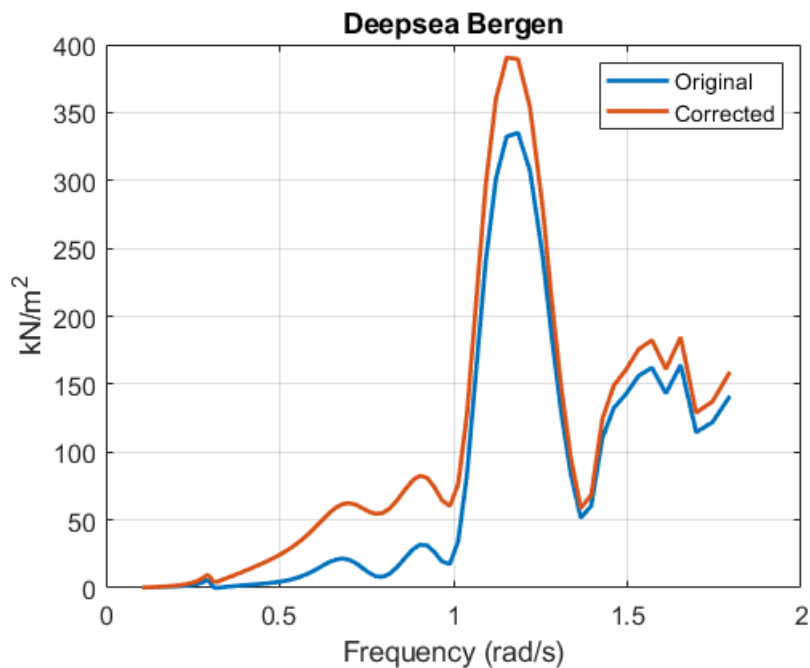


Figure 4-1 Original and corrected wave drift coefficient for surge ($U_c = 0.5$ m/s, $H_s = 7$ m)

5 RESPONSE CHARACTERISTICS OF DYNAMICALLY POSITIONED VESSEL

5.1 Model

To study the dynamic properties of the vessel with dynamic positioning, an 'essential' model was made. The model is linear and has one degree of freedom (dof) of motion. It is *essential* in the sense that it includes the basic characteristics of the vessel mechanics, the DP controller and thruster system.

- The vessel is modelled as separate parts for the low frequency (LF) and the wave frequency (WF) response
 - The LF model is a 2nd-order mass-spring-damper system driven by white noise
 - The WF response is modelled as a narrow-banded process (see below)
- The DP controller uses feedback to the thrusters from estimated LF position error and velocity. The estimator is a Kalman-Bucy filter.
- The thruster system including servo controllers is modelled as one resulting force with a 1st-order lag (time constant)

The model is primarily made for studying impulse response: What will the reaction of the DP system be when a large, sudden excitation occurs. The linearity allows its properties to be investigated in both the time domain and the frequency domain.

- One-dof motion is justified because for a semi-submersible the cross-coupling between the components of motion of the vessel's centre is weak: A force attacking in a given direction will cause a response more or less in the same direction.
- The linearity of the vessel damping – rather than quadratic damping – is justified since the bigger part of the damping comes from the DP system, which is linear

- The thruster response (to the thruster command) will for a real system be nonlinear due to the quadratic hydrodynamic torque resistance. However, the thruster response will also depend on the functioning of the servo system, which is manufacturer-dependent. The basic thruster property to model is the thruster delay, and without further knowledge, a 1st-order lag should be adequate.

The response model is expressed on state space form:

$$\begin{aligned}\dot{\mathbf{x}}_{LF} &= \mathbf{A}_{LF}\mathbf{x}_{LF} + \mathbf{B}_{LF}F_T + \mathbf{B}_{LF}\xi_{LF} \\ \dot{\mathbf{x}}_{WF} &= \mathbf{A}_{WF}\mathbf{x}_{WF} + \mathbf{B}_{WF}\xi_{WF}\end{aligned}\quad (15)$$

Here, the state vectors \mathbf{x}_{LF} and \mathbf{x}_{WF} represent the LF and the WF model, respectively, F_T is thruster force, and ξ_{LF} and ξ_{WF} are "scalar" driving white noise processes.

The elements of the state vector \mathbf{x}_{LF} are LF position and velocity.

$$\mathbf{x}_{LF} = \begin{bmatrix} x_{LF} \\ v_{LF} \end{bmatrix}\quad (16)$$

The matrices \mathbf{A}_{LF} and \mathbf{B}_{LF} are composed as

$$\mathbf{A}_{LF} = \begin{bmatrix} 0 & 1 \\ -k/m & -c/m \end{bmatrix}, \quad \mathbf{B}_{LF} = \begin{bmatrix} 0 \\ 1/m \end{bmatrix}\quad (17)$$

where m is the vessel's total (rigid + hydrodynamic mass) mass, and c the hydrodynamic damping coefficient. For the model to represent horizontal motion (which have no restoring) the stiffness, k , is set to zero. With the parameterization in (17) the white driving noise ξ_{LF} becomes defined as force.

The WF response must have a spectrum that is narrow-banded and concentrated around a peak frequency. This frequency will be close to the peak frequency of the wave spectrum, and the width of the spectrum is expected to be comparable to that of the wave spectrum, as long as the horizontal WF motion is considered.

As a simplification, therefore, the WF motion is modelled as a constant multiplied by the wave elevation:

$$x_{WF}(t) = r_{WF} \eta(t)\quad (18)$$

The coefficient r_{WF} can be regarded as an average RAO across the width of the wave spectrum (It is noted that the purpose of the WF model is to have a basis for the construction of the wave filter used by the controller (Figure 2-1) and not a high-precision model for the WF response).

The Pierson-Moskowitz (P-M) spectrum is found to be a convenient choice of spectrum type since it is readily scalable to any magnitude and location on the frequency axis. To represent the process behind the P-M spectrum as a differential equation, least squares model fitting was used. The method is too involved to be included here but is described in [10] (where it is applied to wind gust spectra). It was found that a model order of six gave an excellent representation of the P-M spectrum, as demonstrated by Figure 5-1. The model was then given state space formulation, cf. Eq. (15), c.f. [10].

The WF state space model was made to represent a normalized P-M spectrum, i.e., the spectrum corresponding to $H_s = 1.0$ and $T_p = 1.0$. Changing the model to represent a different peak period and magnitude of response is easily done by scaling the coefficients in the matrices \mathbf{A}_{WF} and \mathbf{B}_{WF} .

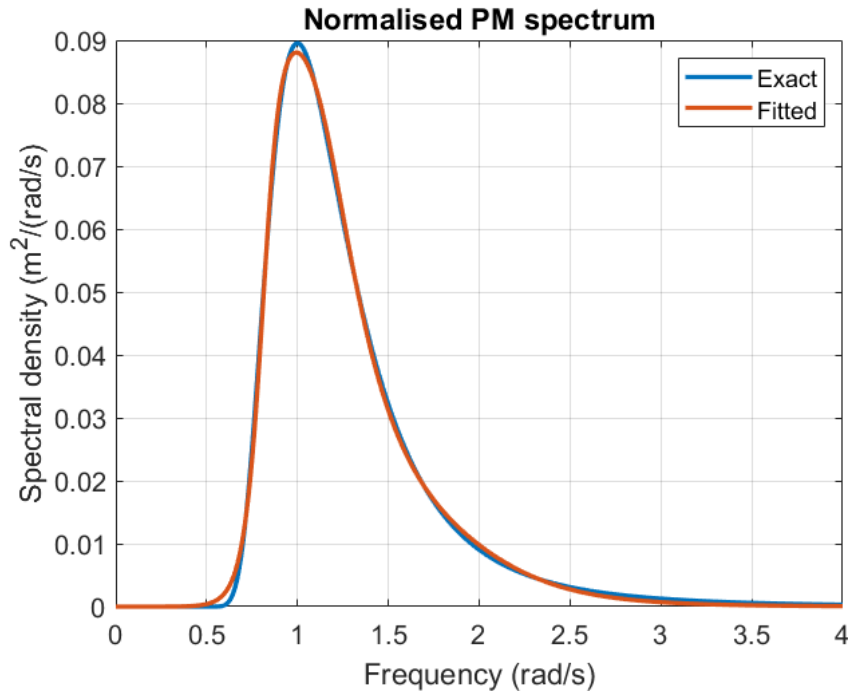


Figure 5-1 The spectrum corresponding to the 6th order model for WF motion in comparison with the Pierson-Moskowitz spectrum .

The main input to the controller is the measurement of position, which is modelled as the sum of LF and WF position:

$$y = \mathbf{C} \begin{bmatrix} \mathbf{x}_{LF} \\ \mathbf{x}_{WF} \end{bmatrix} + w \quad (19)$$

Here, the vectors of LF and WF position form a combined state vector of eight components. The variable w is measurement noise. \mathbf{C} is a constant measurement matrix that maps the right state variables to the (scalar) measurement, y (The 3rd WF state is the wave elevation, the other five states are auxiliary variables):

$$\mathbf{C} = [1 \ 0 \ 0 \ 0 \ 1 \ 0 \ 0 \ 0] \quad (20)$$

Eq. (19) and the model (15) are the basis for the design of the state estimator (observer). Its task is to make an estimate of the LF state, $\mathbf{x}_{LF} = [x_{LF}, v_{LF}]^T$ given the measurement, y . In addition to the coefficients of the matrices in the state space model, the (constant) power densities of the process noises (ξ_{LF} and ξ_{WF}) and the measurement noise (w) must be known.

For the state estimation, the Kalman-Bucy filter is used. This filter is the continuous time equivalent of the better known Kalman filter. The details of the estimator are not given here but can be found in [11] or elsewhere in the rich literature on the subject.

When the estimate ($\hat{\mathbf{x}}_{LF}$) of the LF state is obtained, the feedback command to the thrusters is expressed as

$$u = -\mathbf{G} \hat{\mathbf{x}}_{LF} \quad (21)$$

where the gain matrix \mathbf{G} consists of position gain and velocity gain:

$$\mathbf{G} = [g_p \quad g_v] \quad (22)$$

To model the response of the force (F_T) from the thrusters a simple 1st-order model is used, as mentioned above:

$$\dot{F}_T = -\frac{1}{T_T} F_T + \frac{1}{T_T} u \quad (23)$$

This equation represents the combined response of the thruster dynamics and the thruster controller. The quickness of the response is determined by the time constant T_T , see Figure 5-2, which shows the thruster response to a unit step in the commanded thrust. After a time, equal to the time constant, the thrust has reached 63 % of its final value.

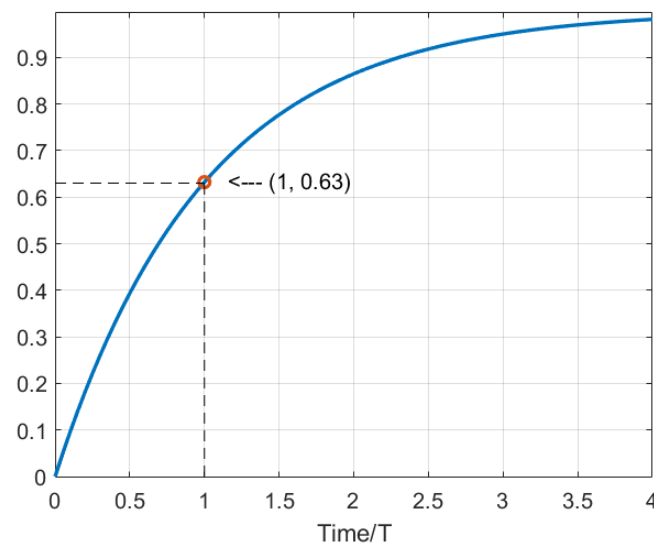


Figure 5-2 Unit step response corresponding to the first-order model in Eq. (23) . T is the time constant.

5.2 Example

5.2.1 Model data

The frequency response and impulse response of the system described above are calculated using data for Deepsea Bergen. The Kalman-Bucy filter was based on the sea state $H_s = 7$ m, and $T_p = 9.1$ s and the assumption of P-M spectrum. The parameters used in the calculation are summarized in Table 5-1. The data pertain to the semi's surge motion.

Using the spring-mass-damper analogy in Section 3.1 the gains of the controller were chosen such that the bandwidth of the controller becomes 1/100 Hz and the damping ratio about 0.7, including the effect of the natural hydrodynamic damping. Using the frequency domain program MIMOSA, the standard deviation of the LF and WF motions were calculated as 1.84 m and 0.40 m, respectively. The standard deviation of LF motion was obtained by the above model (15) by choosing the power density of the driving white noise, V_{LF} , listed in the table. The value $r_{WF} = 0.23$ to give the wanted WF standard deviation of 0.40 m, is close to the

true RAO value (≈ 0.21) at the peak period ($T_p = 9.1$ s) of the wave spectrum. This supports the reasoning behind Eq. (18).

Table 5-1 Vessel and DP parameters used in example

Vessel total mass (surge)	m	29945	tonnes
Vessel damping coefficient	c	180	kN/(rad/s)
Power density of LF driving noise, ξ_{LF}	V_{LF}	9.0E+05	(kN) ² /(rad/s)
Coefficient of WF response model	r_{WF}	0.23	m
Power density of measurement noise	W	0.25	m ² /(rad/s)
Controller position gain	g_p	120	kN/m
Controller velocity gain	g_v	2473	kNs/m
Thruster time constant	T_T	10	s

5.2.2 Filter characteristics

With the parameters in Table 5-1, the frequency response of the Kalman-Bucy filter is shown as a Bode plot in blue in Figure 5-3. The graphs show the frequency response from position measurement to LF position. The curves in red show the case when there is negligible WF motion. The purpose of the filter in this case is to filter off measurement noise. The difference between the two filter characteristics is that the blue amplitude curve contains a "trench" in the frequency range of the WF response. The amplitude value of the trench is about -13 dB, which corresponds to a reduction of 4.5 times as compared to the zero-frequency amplitude ($= 0$ dB) (It is noted that this filter, based on the Kalman-Bucy theory, is the best obtainable filter, given the premises). Figure 5-4 shows the characteristic of the filter in linear axes.

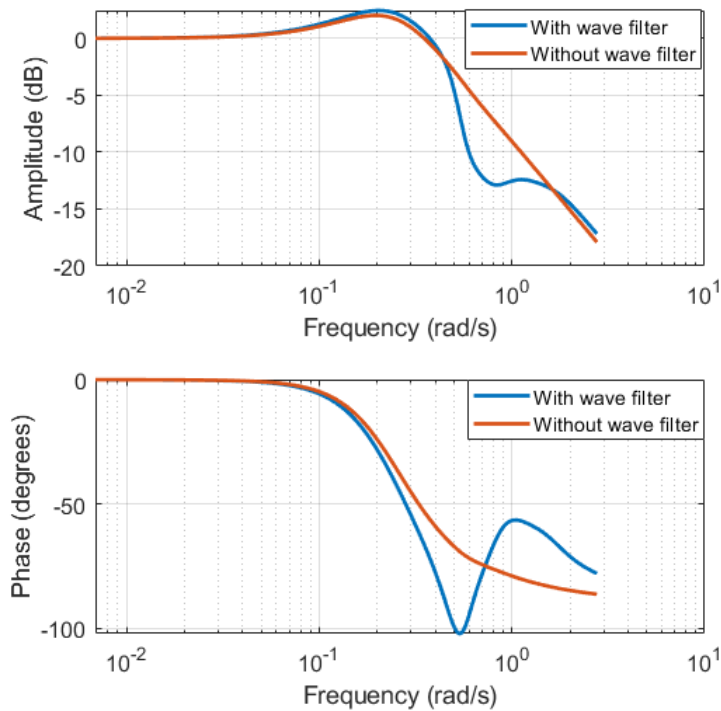


Figure 5-3 Bode plot of Kalman-Bucy filter for LF position

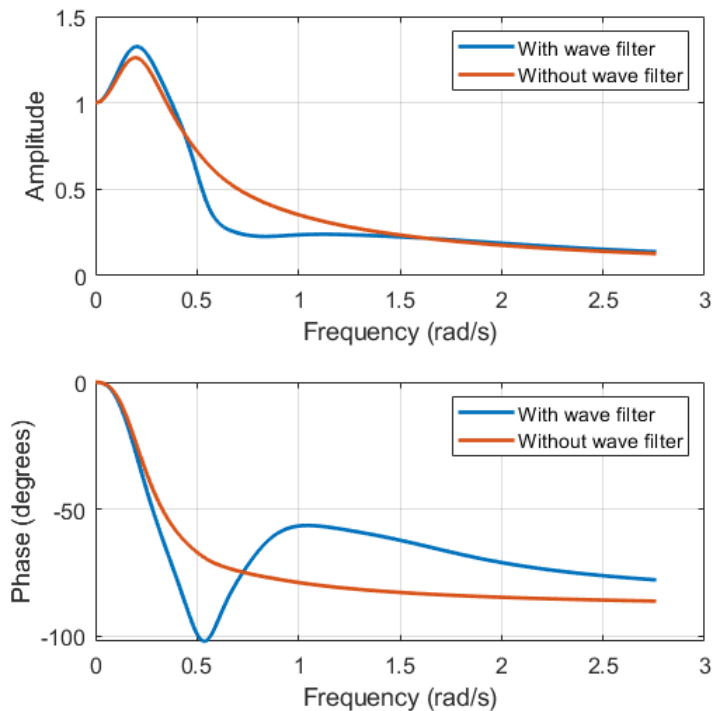


Figure 5-4 Characteristic of Kalman-Bucy filter. Same as above figure, but in linear axes.

5.2.3 Response of dynamically positioned vessel

5.2.3.1 Response with and without thruster delay

With the parameters in Table 5-1, the frequency response of the vessel with DP system is shown in Figure 5-5 (only the amplitude response is shown). The figure shows the position response amplitude caused by a load of unit amplitude. The ordinate axis is scaled in dB, but the underlying unit is m/kN. The figure shows the response without and with thruster delay (= 10 seconds as in Table 5-1). The increase (= deterioration) of the response when the reaction time of the thrusters is included is clearly seen.

Comment 1: The choice of controller gains as described in Section 5.2.1 was based on simple mass-damper-spring analogy without consideration of thruster delay. It is likely that a more thorough choice of gains would reduce the resonance peak of the blue curve in Figure 5-5.

Comment 2: The frequency response would normally be expected to approach zero towards zero frequency, but this requires that an integrator be included in the DP controller. Since the purpose of the model is to study impulse response, the slow action of an integrator will have no effect.

The impulse response with and without the 10 seconds thruster delay is shown in Figure 5-6. In the calculation an impulse of 10 000 kNs is used. Maximum excursion and thruster force are shown in Table 5-2. Again, the reaction time of the thruster causes a bigger response.

Table 5-2 10 000 kN impulse - maximum excursion and thruster force

Thruster time constant, T_T (s)	Excursion maximum (m)	Force maximum (kN)
10	5.2 m	761
0	4.0 m	743

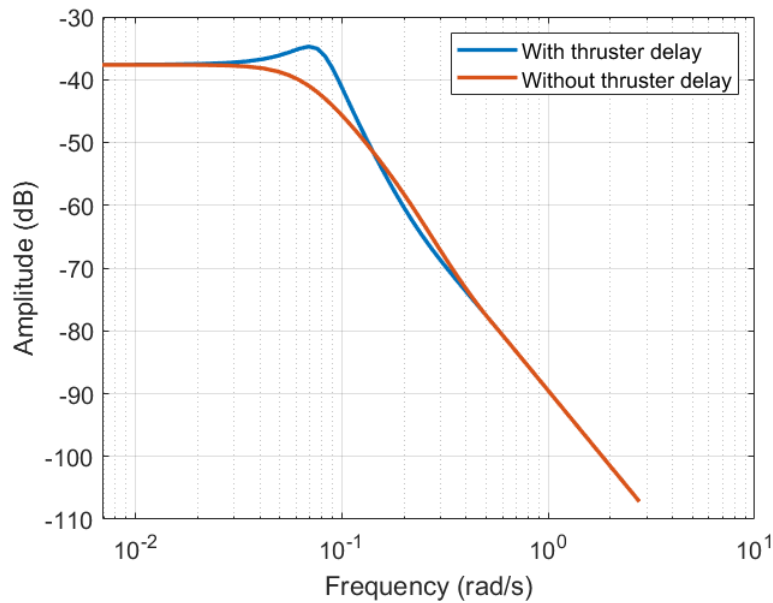


Figure 5-5 Frequency response of transfer function from LF load to LF position response

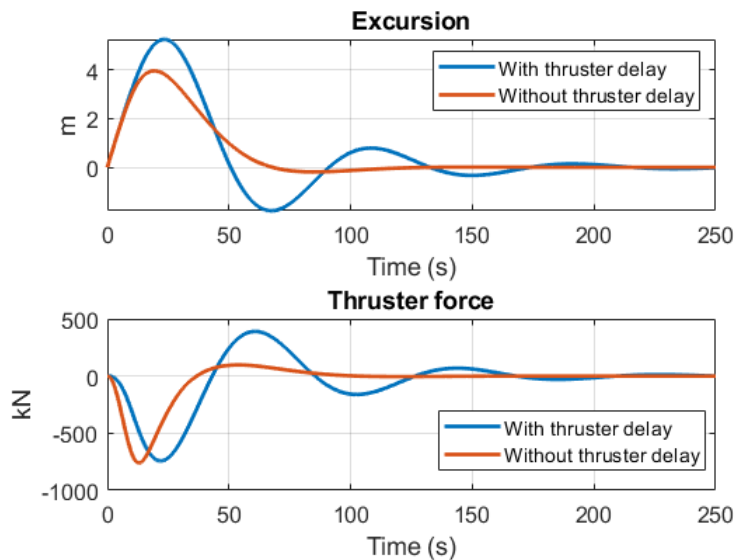


Figure 5-6 Impulse response with and without thruster delay (Time constant of 10 s)

5.2.3.2 Analysis of impulse response

A reflection on the impulse response in Figure 5-6 indicates that the vessel excursion is significantly larger than indicated by the simple analysis of the mass-damper-spring model in Section 3.1. The cause of this must be 1) the filter delay, and 2) the thruster delay. To study the effects of these two delays, the simplified numeric model was excited with the impulse load $I_1 = 29\,000$ kNs, which resulted in a maximum excursion of 7 m for the delay-free model in Section 3.1, cf. Eq. (5).

Figure 5-7 shows the position response of the vessel when subjected to the impulse I_1 (red line). The maximal excursion is 15.2 m, which is more than twice that of the delay-free mass-damper-spring model in Section 3.1, which is shown in blue and designated "Ideal" in the legend box. The causes of the difference are as pointed out, the lags in the state estimator (filter) and the thruster response. The former is seen from the yellow line in the figure, which shows the estimated position. The position feedback of the controller is based on this variable.

A clearer illustration is given by Figure 5-8. This figure shows the velocities that correspond to the positions in the former figure. An (ideal) impulsive load gives an instantaneous change in velocity. According to the figure, the load I_1 gives a start velocity of almost 0.9 m/s both in the ideal (=lag-free) case and the true (or actual) case. The *estimated* velocity – which is calculated from the position measurement by the Kalman-Bucy filter in the DP controller – begins at zero and needs some time to converge to the true velocity. In the ideal case, the damping force takes effect immediately and starts slowing down the excursion at once. In the actual case, the damping is obtained from the *estimated* velocity and needs some time to take full effect. This is what causes the difference between the red and blue curves in Figure 5-7 and Figure 5-8.

To find out which effect is the greater – the delay in the filter, or the delay in the thruster response – the above calculation is repeated with a thruster time constant of $T_T = 1$ s, which gives an almost immediate thruster reaction. The result is shown in Figure 5-9 and Figure 5-10. The maximum position deviation is now 11.4 m, which is still significantly higher than the 7 m maximum in the ideal case. This difference is due to the lag in the wave + noise (Kalman-Bucy) filter.

Comment: One might surmise that the "ideal" response, i.e., the response of the mass + damper + spring model could well represent that of a mooring system. However, the model has a damping ratio of 70 %, which is representative of a DP system and not obtainable for a mooring system.

Turning to the slamming case in Section 3.1 and the estimated slamming load $I_2 = 5000$ kNs. This load will cause an excursion maximum of 2.4 m when the filter and thruster delays are considered (vs. 1.2 m in the ideal case). Note that this excursion is a real estimate linked to a sea state and vessel dimensions, whereas the values in the above figures originate from the original, random choice of 7 m as the maximum excursion. Nevertheless, the examples show the effect of the delayed control action.

It is expected that the importance of quick regulator action is less when the disturbing load has longer duration. To check this, the model was excited with rectangular pulses of varying duration, but equal impulse value (i.e. magnitude times duration). The impulse value was chosen equal to $I_1 = 29\,000$ kNs. In Figure 5-11 to Figure 5-13 the case with an ideal impulse from the example in Figure 5-7 and two cases of longer pulses are shown (20 seconds and 60 seconds, respectively). Position response and thruster force are shown.

The peak values of vessel position and thrust are shown in Table 5-3. For the pulse of 20 seconds length the peak of the excursion is not much less than for the ideal impulse. In the case when the pulse length is 60 seconds the maximum excursion is almost as low as the maximum in the case of a delay-free control system.

These results show that the DP system acts as intended by design: short disturbances are supposed to pass unrestrained. The problem arises when the disturbance has the character of a short-lasting strong transient load, rather than a cyclic load at wave frequencies.

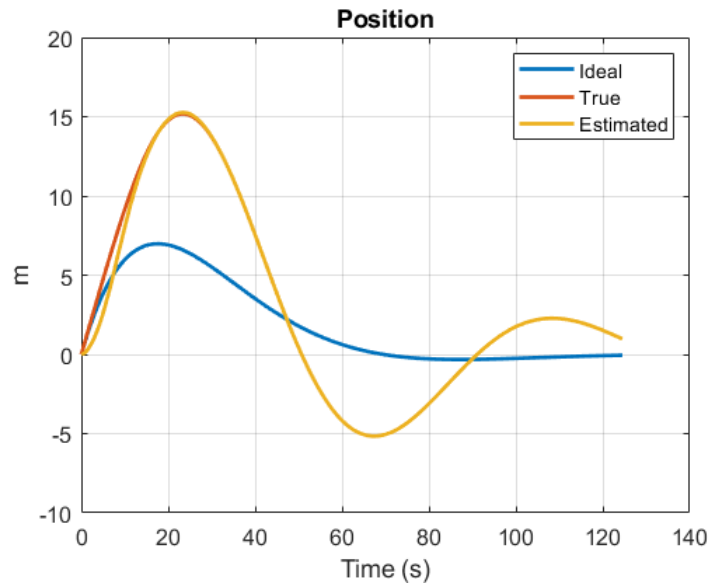


Figure 5-7 Impulse response of position. $T_T = 10$ s

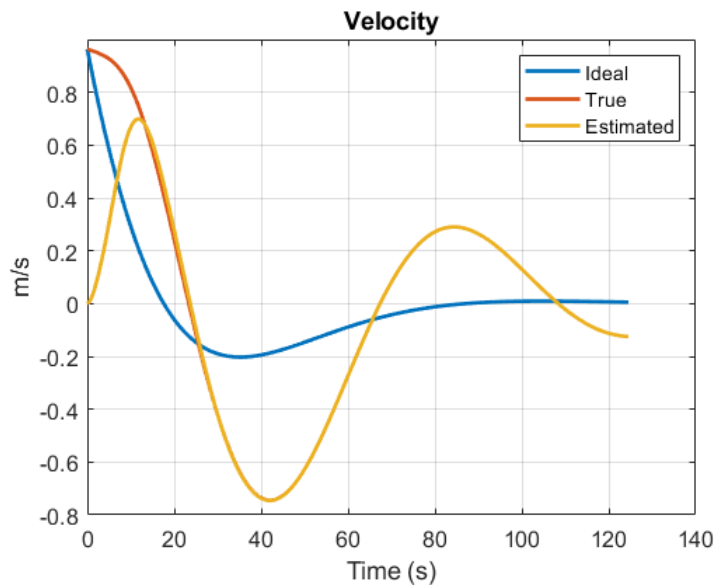


Figure 5-8 Impulse response of velocity $T_T = 10$ s

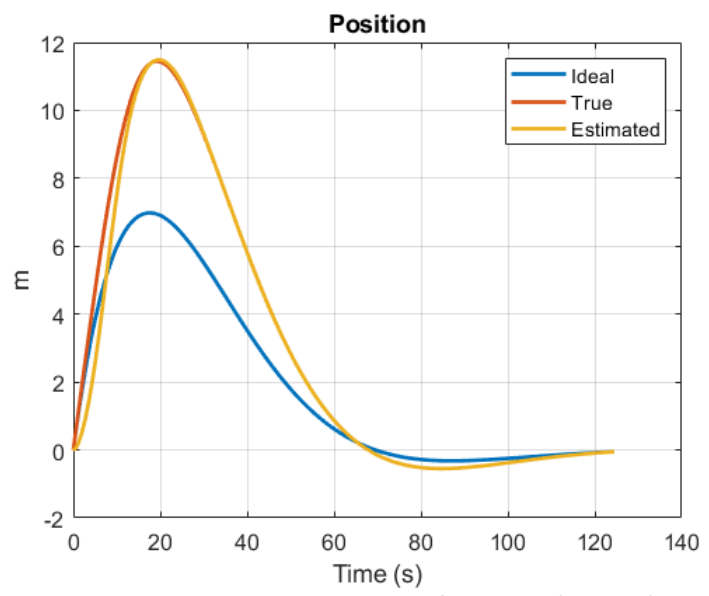


Figure 5-9 Impulse response of position ($T_T = 1$ s)

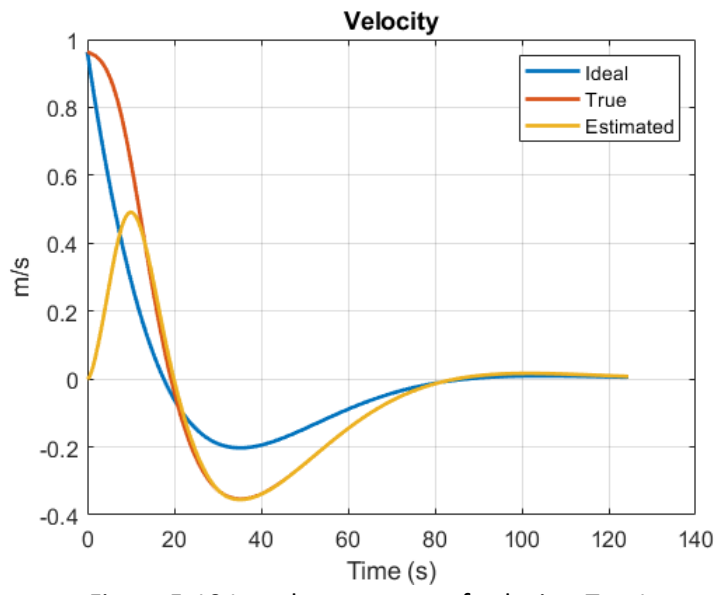


Figure 5-10 Impulse response of velocity, $T_T = 1$ s

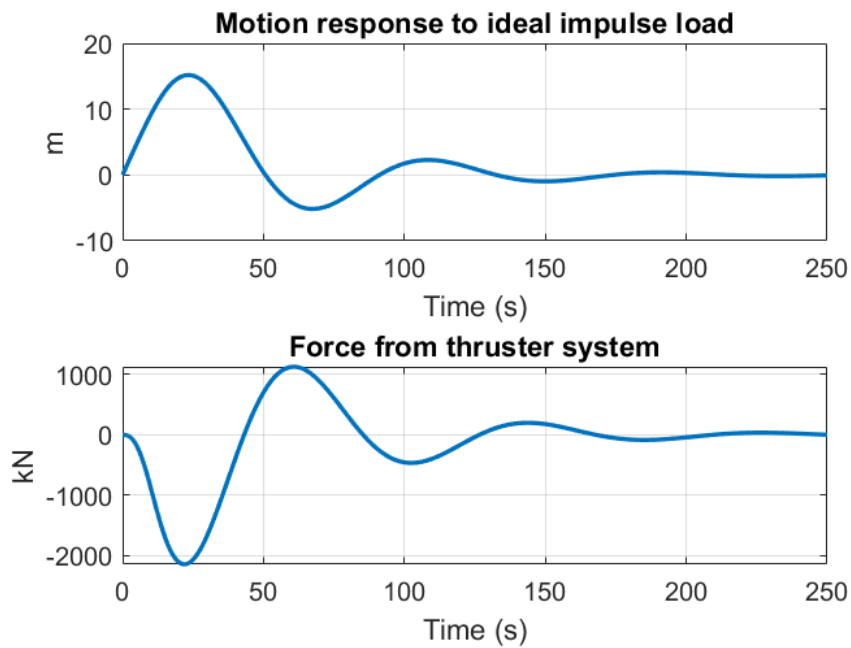


Figure 5-11 Position and thruster force in case of ideal impulse load

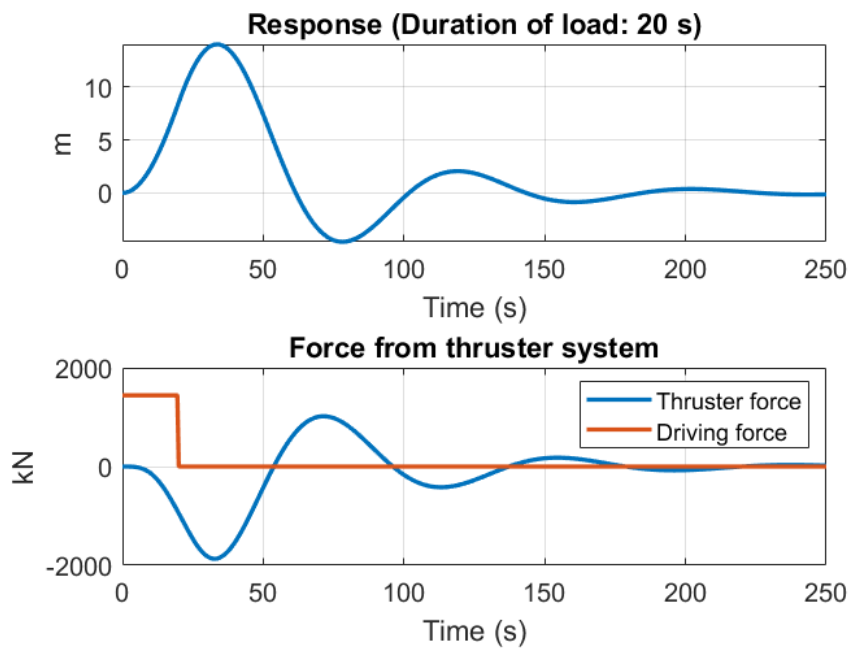


Figure 5-12 Response to a rectangular pulse of 20 seconds length

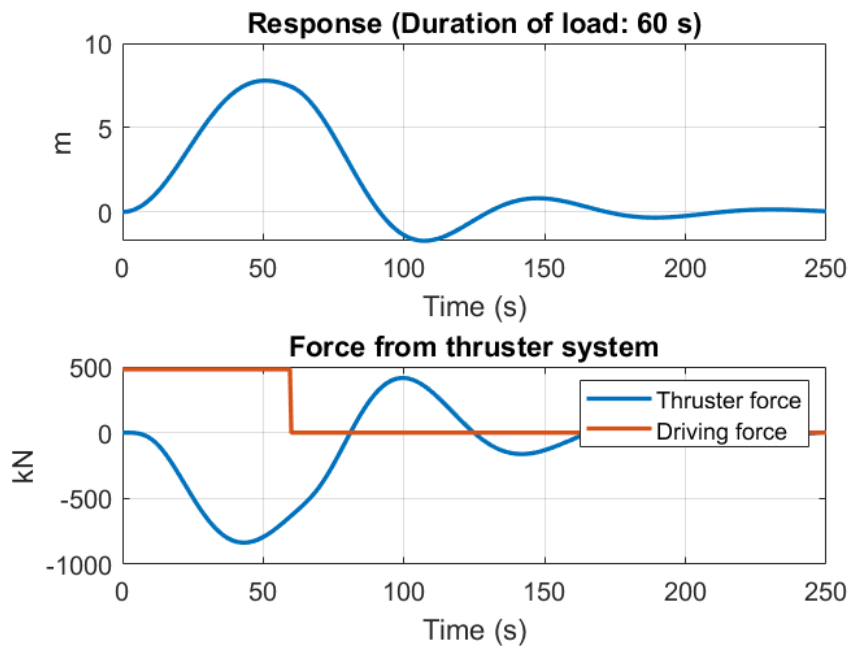


Figure 5-13 Response to a rectangular pulse of 60 seconds length

Table 5-3 Maxima of position and thruster force for different pulse lengths

	Ideal impulse	Pulse length 20 s	Pulse length 60 s
Position peak	15.2 m	14.0 m	7.8 m
Force peak	-2126 kN	- 1865 kN	- 836 kN

5.2.3.3 Importance of the initial state

In the previous paragraph, an excursion peak of 2.4 m was found for the slamming event described in Section 3.1 when the delays in the DP system were included in the calculation. The assumed wave condition of $H_s = 7$ m and $T_p = 9.1$ s represents a condition of steep waves and has an expected return period of one year. In the load calculation the wave that caused the slamming load was assumed to form a vertical wall immediately before hitting the columns of the semisubmersible vessel. The probability of such a wave arising at all and in addition doing so right in front of the vessel is unknown, but probably tiny.

Another factor of importance is the motion state of the vessel when the wave hits. An ideal impulse will cause an immediate change in the velocity of the vessel. The calculations above are carried out for the case when the velocity of the vessel is zero. However, the velocity may be negative when the load happens, which may retard the vessel and reduce its kinetic energy. Equally well, the velocity may be positive in the slamming instant and made to increase further by the load. It may also happen that the vessel is close to the offset limit when the wave hits and is driven across it by the load. To carry out a probabilistic study of these cases is interesting, but beyond the scope of the present study.

6 SIMULATION OF MOTION IN IRREGULAR SEA

6.1 SIMO model

In irregular sea, characterized by a wave spectrum, the vessel motions will be irregular too. The peaks of motion will be random and vary in magnitude. When the duration of the simulation is long enough, a reliable statistical distribution of the peaks can be calculated.

(The motion will consist of a combination of 1st order components generated by a linear response model and slowly varying components generated with a 2nd-order model. The spectral range of the 1st order response is the same as the range of the wave spectrum and the 1st-order response is therefore frequently referred to as *wave frequency* or *WF* response. The 2nd order response components are the result of non-linear frequency mixing and will contain frequencies across a broad range. However, usually only the low frequency (LF) components are significant.)

To see what response peaks one must expect under stationary conditions, simulations were carried out with SINTEF Ocean's simulation code SIMO [12]. To calculate the wave-drift loads, Newman's method was used, cf. Section 3.3. To include viscous effects on the vessel's columns and the effect of current the correction formula (14) from the Exwave project [8] was used.

Two numerical models were used, one representing Deepsea Bergen (Figure 6-1), the other the "Exwave semi" (Figure 6-2).

Comment: As shown by the figures, the two semis have columns of different cross-sectional shape, i.e. circular and square. This was a criterion for the choice of the models, as it was initially assumed that large slamming load might be a cause of position loss, and that the magnitude of the load might depend on the geometry of the columns. However, as discussed in section 3.1, the magnitude of the slamming impulse is moderate. Slamming is therefore not expected to be a single cause of loss of position, whatever be the shape of the columns. Another indication of the unimportance of the columns' cross-sectional geometry is the fact that the correction formula (14), which is based on empirical data, requires no information about it.

Table 6-1 Main particulars of the two semis

Parameter	Deepsea Bergen	Exwave semi
Length of pontoons	92.5 m	107.5 m
Width	67.2 m	81.3 m
Draught (survival)	17.5 m	23.0 m
Displacement (survival)	25 963 t	39 206 t
Radii of gyration:		
roll	29.4 m	36.1 m
pitch	31.3 m	34.4 m
yaw	35.0 m	42.3 m
Width of columns	9 m and 7.4 m (circular)	12.5 m (square)

The original SIMO model data from the Exwave project for the two semis include:

- Structural mass and moments of inertia
- Added mass matrix

- Hydrostatic and gravitational restoring matrix
- Wave-to-motion transfer functions
- Wave-to-force wave drift coefficients
- Linear and quadratic damping coefficients
- Quadratic current load coefficients
- Mooring system

The models did not include a DP system, so the mooring system model was removed and replaced by a "generic" DP system. The DP controller in SIMO uses PID control based on state estimates from a quasi-Kalman observer. The thruster dynamics are modelled by coefficients of thrust and torque, rotational inertia, and servo controller. Both fixed-direction and rotatable (azimuth) thrusters can be modelled.

For the study, four identical azimuth thrusters were modelled. The basic controller and thruster data are shown in Table 6-2. The gains of the DP controller are functions of the bandwidth and damping ratio. The intention was to make the DP system in SIMO similar to the DP system of the simplified model in Chapter 5. However, due to a lapse the controller for Deepsea Bergen was chosen a bit stiffer, as shown the table. The coefficients of the filter are also functions of the chosen bandwidth and damping ratio. The filter characteristic is consequently not based on assumptions of the power spectral densities of process noise and measurement noise as was the basis for the Kalman-Bucy filter used above. The adaptive wave filter in SIMO is a harmonic oscillator with time-varying frequency of oscillation and amplitude that are estimated simultaneously with the ordinary state variables. It is assumed that this filter *in average* will behave like the filter used in the simplified model.

Table 6-2 DP data

Parameter	Deepsea Bergen	Exwave semi
Controller bandwidth	1/77 Hz	1/100 Hz
Controller damping ratio	70 %	70 %
Filter bandwidth	1/30 Hz	1/30 Hz
Filter damping ratio	70 %	70 %
Rise time of thrusters	14 s	14 s
Capacity of thrusters	Sufficient	Sufficient

The simulations are done with excitation in the vessels' surge direction. Due to symmetry, there will be negligible sway and yaw motion, and the thrusters will be directed along the vessel's surge axis. To avoid loss of efficiency when a thruster needs to turn 180° to give thrust in the opposite direction, the limit on the turning rate is set very high. This is unrealistic but will model the case when the thrusters are set in biased mode or locked at fixed angles.

The rise time in Table 6-2 is the minimum time the thruster needs to go from 10 % to 90 % of full capacity. Unlike the linear model (23) the model for thruster dynamics in SIMO is nonlinear. The rise time of 14 s in the table is assumed to have the same effect as the time constant $T_T = 10$ s in Table 5-1 (However, no thorough comparison has been carried out).

The force capacity of the thrusters was set sufficiently high to prevent the thrusters from saturating.



Figure 6-1 The Deepsea Bergen: numeric and physical model

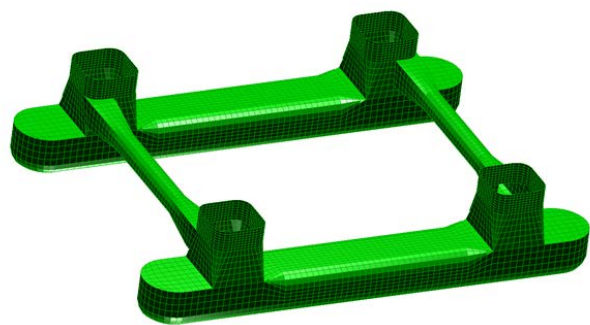


Figure 6-2 The Exwave semi

6.2 Sea states

For the simulations with SIMO, five sea states of moderate significant height were selected. The sea states represent conditions of steep waves: the peak periods are chosen from the 1-year contour line for the Haltenbanken in The Norwegian Sea (Figure 6-3), as calculated from the Nora 10 metocean data base [14]. Thus, each state has a mean return period of one year. Simulations are carried out for five sea states, all having the JONSWAP spectral shape. The parameters of the sea states are shown in Table 6-3. The sea states are moderate with respect to height and may - considering wave height alone - well represent normal off-shore operation conditions. The values of γ in the table are the typical values that correspond to the significant wave height and the peak period.

In addition to waves, a current of speed 0.5 m/s in the direction of the waves is used. Wind gusts are expected not to contribute significantly to the dynamic motion of the vessels and is not modelled.

Table 6-3 Sea states

Significant wave height H_s (m)	Peak period T_p (s)	Peakedness parameter γ
5.0	7.1	5.0
6.0	8.1	5.0
7.0	9.1	5.0
8.0	10.1	5.0
9.0	11.2	4.3

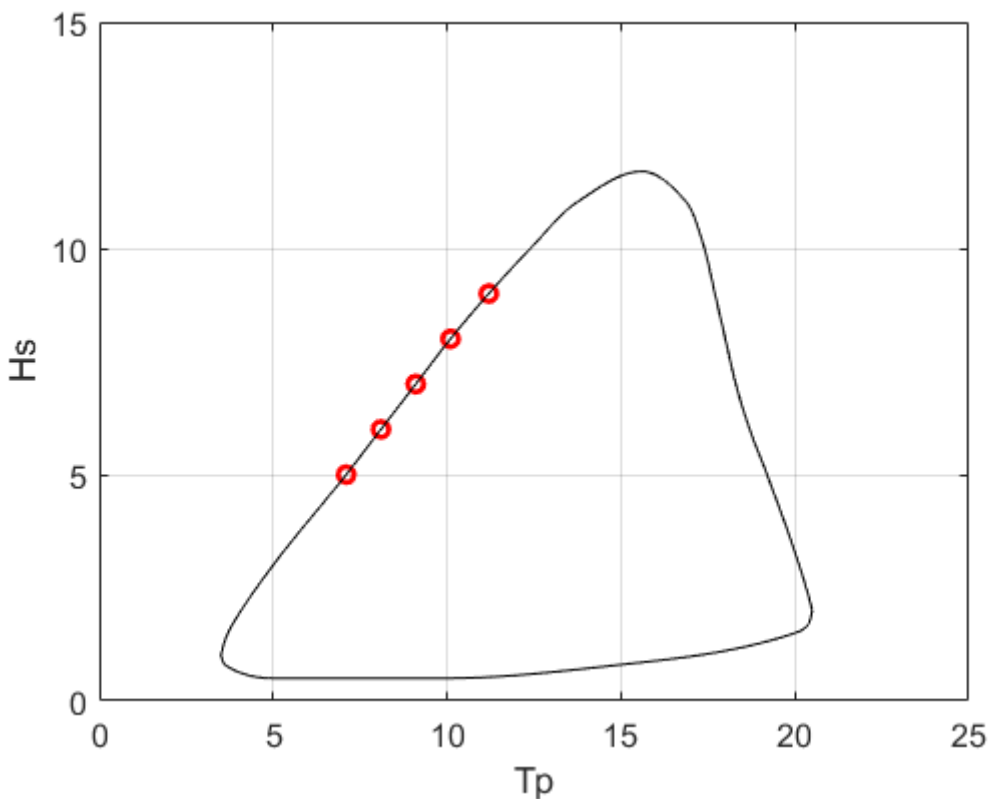


Figure 6-3 Sea states used in the simulations. These states lie on the 1-year contour line.

For each sea state the wave-drift coefficients are modified according to the formula (14). In addition, wave-drift *damping* coefficients are estimated from the material in the Exwave Joint Industry Project, see Table 6-4. The damping coefficients depend on the sea state. They were calculated for a common γ value of 3.3 and not the values in Table 6-3, but this is considered not to introduce significant error in the simulations (considering that the damping from the DP system is one order of magnitude greater).

Table 6-4 Wave-drift damping coefficients

H_s (m)	T_p (s)	Wave drift damping coefficient (kN s/m)	
		Deep Sea Bergen	Exwave semi
5.0	7.1	187.6	232.0
6.0	8.1	229.1	166.9
7.0	9.1	254.4	233.8
8.0	10.1	247.5	320.1
9.0	11.2	267.3	312.9

6.3 Simulations

For each semi and each sea state, simulation runs were carried out with three hours duration plus time for initial transients to settle. For the Deepsea Bergen some parameter variation has been carried out in order to check which metocean parameters are important.

6.3.1 Parameter variation

In addition to the sea states in Table 6-3 some simulations with the model for Deepsea Bergen were carried out to check the motion response's dependence on various parameters. The simulated duration is three hours. The results are presented in a qualitative way as cumulative distribution plots with fitted Weibull distribution. The following "base case" was chosen:

$$H_s = 7 \text{ m}, T_p = 9.1 \text{ s}, \gamma = 5, U_c = 0.5 \text{ m/s}, C_p = 0.25 \text{ s/m}$$

Here, U_c is the current speed and C_p is the current coefficient in the Exwave correction formula (14).

To check the importance of wave steepness, the peak period associated with $H_s = 7 \text{ m}$ was changed to the statistically expected value, $T_p = 13 \text{ s}$, see Figure 6-4. The cumulative distribution of LF + WF surge motion for this condition is shown with that for the base case in Figure 6-4. The two curves cross at $x = 3 \text{ m}$ and consequently have the same probability of exceedance (or non-exceedance) at this point. Below this value the "normal" wave state gives surge response of higher probability than the "steep" wave state. Above 3 m the opposite happens. The explanation for this is that the peak period of 13 seconds gives larger WF response than the 9.1 seconds peak period, whereas the LF response dominates for the latter. For the two cases, the sample maximum is $x = 7.6 \text{ m}$ for the steep case and $x = 12.9 \text{ m}$ for the normal case. Hence, from this example, it appears that wave steepness has a significant effect on the extreme surge response.

To see the effect of swell, a swell condition of 2 m H_s and 15 s T_p was superimposed on the base case. As shown by Figure 6-5 the existence of swell has no noticeable effect on the extremes. This agrees with Figure 3-4, which shows there is almost no wave drift force generated at low wave frequencies.

The effect of the Exwave correction is demonstrated in Figure 6-6. As is seen, the effect is tremendous. The sample maximum increases from 5.5 m to almost 13 m when the formula is applied. The figure also shows the contribution of the "potential correction" when current is present. This effect is determined by the coefficient C_p in Eq. (14). Without this effect ($C_p = 0$), the curve in the figure is raised somewhat (blue points → red points), but most of the distance to the non-corrected curve of green points remains. This indicates - at least in this example - that the largest correction given by the Exwave formula is due to viscous effects.

Comment: The values of cumulative probability could have been shown in logarithmic axis to express better the distribution of points close to the upper probability limit of 1. However, the

graphs were obtained from the workbench and user interface Sima, which does not yet offer this as an option.

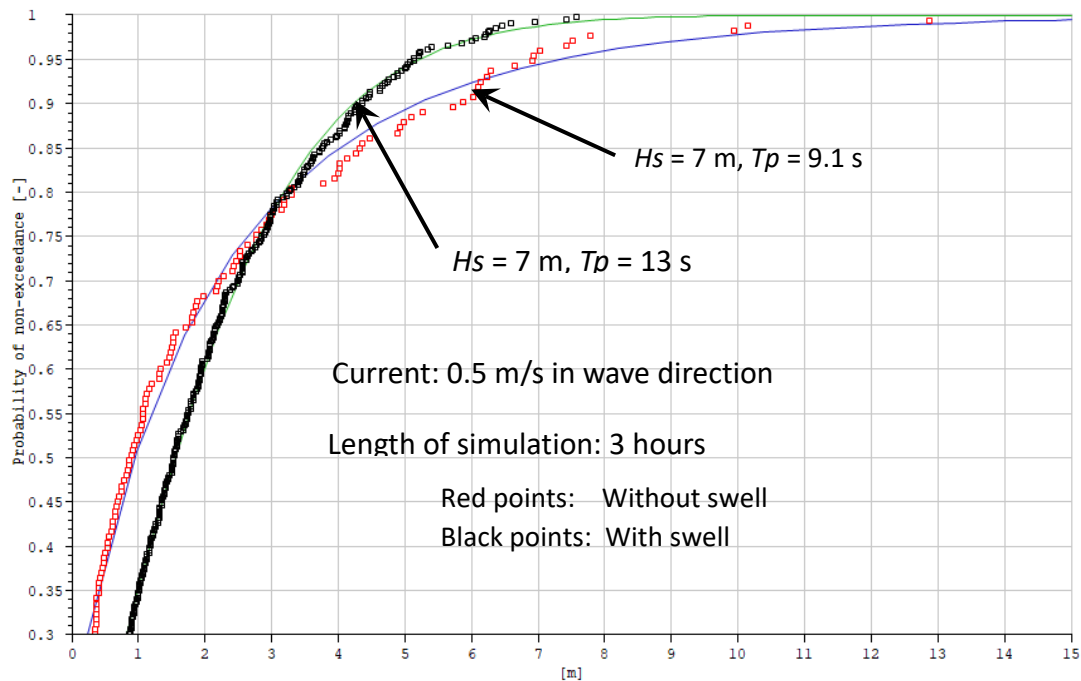


Figure 6-4 Cumulative distribution of simulated LF+WF surge response with fitted Weibull distribution. The red points represent the base case of step waves, the black points represent a case of statistically expected or *normal* steepness.

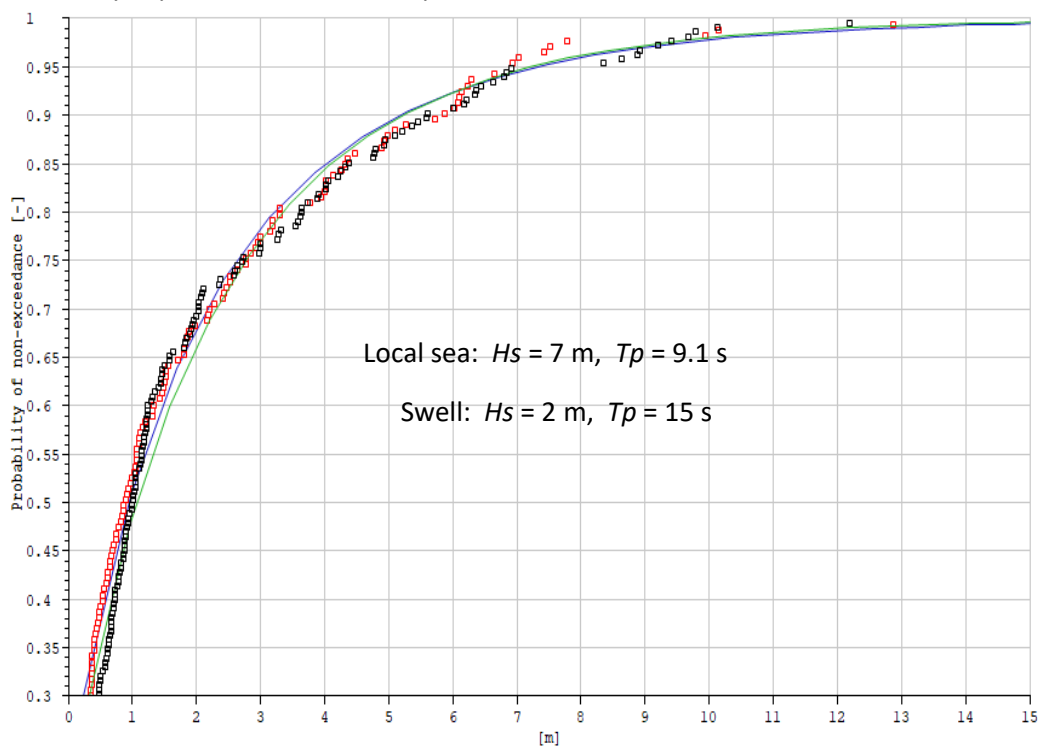


Figure 6-5 Distribution of surge motion with (red points) and without swell (black points) in addition to local sea.

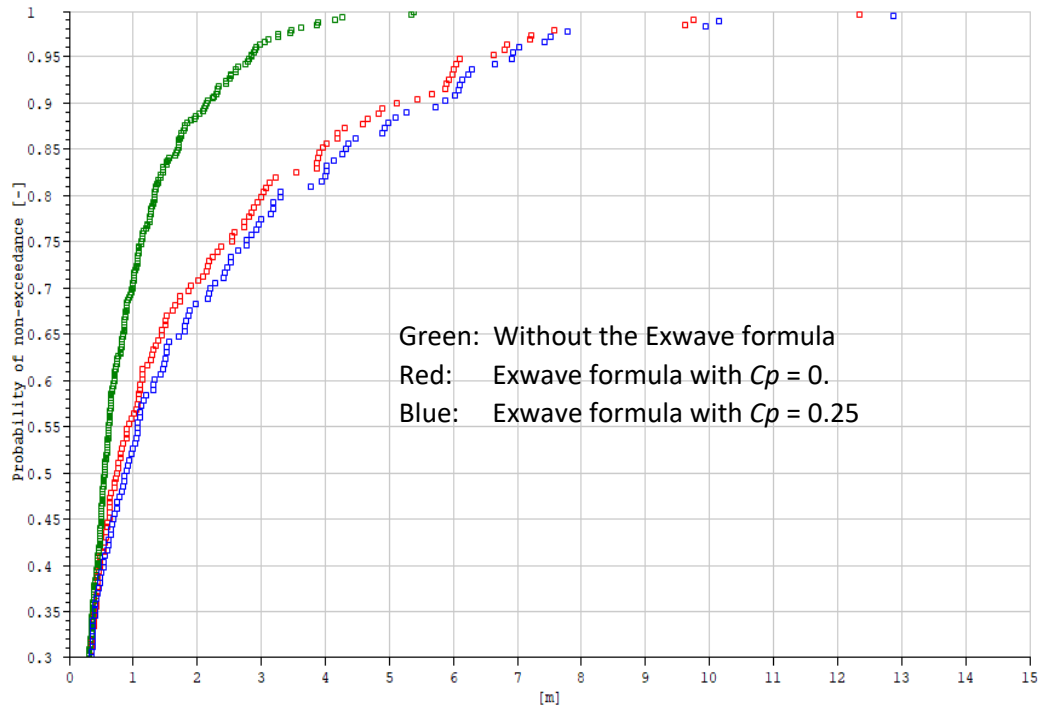


Figure 6-6 Cumulative distributions showing the effect of the Exwave formula. $C_p = 0$ gives only viscous correction. $C_p = 0.25$ gives potential correction in addition.

6.3.2 Simulation results

6.3.2.1 Deepsea Bergen

Three-hour simulations were carried out for the Deepsea Bergen for the five sea states in Table 6-3. The Exwave formula was used with $C_p = 0.25$ s/m and the wave-drift damping coefficients in Table 6-4. The travel direction of the waves was along the vessel's surge axis. A current speed of 0.5 m/s was used in the same direction, which contributes to increase the wave drift force.

Statistics for the surge motion and LF force are shown in Table 6-5. For the motion, the standard deviations of the WF and LF parts are shown separately in addition to the standard deviation of the total (WF+LF) motion. For the calculation the LF and WF responses were derived from the total response by low-pass and high-pass filtering. As shown by the table, the LF motion is strongly predominant for all the sea states.

The minima and maxima are sample values, i.e. the extremes that occurred in the simulations. The sample minima of wave-drift surge force are zero for all wave states. This is as expected from Newman's approximate method. *Ratio* in the table is defined as

$$Ratio = \frac{\hat{x} - \bar{x}}{\sigma} \quad (24)$$

where \hat{x} , \bar{x} and σ denote the maximum, the mean and the standard deviation, respectively. For the Wave-drift force in the table, *Ratio* lies between 7.1 and 9.0, which reflects the fact that the force is exponentially distributed. For the surge motion, *Ratio* lies between 4.3 and 5.2, which indicates that the distribution of

surge offset tends toward the Gaussian distribution. Still, the maxima are much higher than those one would expect from the Rayleigh distribution. The variation in the values of *Ratio* from one wave state to the next may not be significant, since the sample maximum is known to have a large statistical spreading. Statistical uncertainty may therefore be the likely explanation for the fact the maxima of motion and force for $H_s = 8$ m are greater than those for $H_s = 9$ m.

Ratio is a crucial parameter. In cases when the basic measure of response is standard deviation, extremes – such as the expected maximum or the most probable maximum in a given period of time - are usually estimated by applying a factor such as *Ratio* to the standard deviation. The value of the factor depends on the assumption of the underlying statistical distribution. For WF response extremes, the extremes are well estimated from the assumption that the response peaks be Rayleigh-distributed. For a period of three hours this usually leads to values in the range 3.7 - 3.9. For the LF extremes, estimation is much more complicated and usually gives higher values of *Ratio*, cf. [13] and [16].

Comment: Since the surge response is the sum of WF and LF response, one will expect *Ratio* to lie between the values that can be expected for WF motion and LF motion separately. In Table 6-5 *Ratio* is well above the expected Rayleigh estimate of 3.7-3.9. This shows that estimation of extremes based on the Rayleigh assumption should not be used when the response is partly caused by wave drift.

Table 6-5 Statistics for Deepsea Bergen. Three-hour simulations with sea states in Table 6-3

		$H_s = 5$ m $T_p = 7.1$ s	$H_s = 6$ m $T_p = 8.1$ s	$H_s = 7$ m $T_p = 9.1$ s	$H_s = 8$ m $T_p = 10.1$ s	$H_s = 9$ m $T_p = 11.2$ s
Surge position (m)	Mean	0.00	0.00	0.00	0.00	0.00
	St. dev. WF	0.15	0.19	0.35	0.56	0.75
	St. dev. LF	1.49	1.58	2.14	2.67	2.85
	St. dev. total	1.51	1.61	2.19	2.77	3.02
	Minimum	-2.86	-3.22	-4.72	-6.22	-7.11
	Maximum	6.97	6.85	11.44	13.48	12.94
	Ratio	4.6	4.3	5.2	4.9	4.3
Wave-drift force in surge (kN)	Mean	301	352	436	499	529
	Standard dev.	310	356	436	496	525
	Minimum	0	0	0	0	0
	Maximum	2943	3410	4377	4371	4253
	Ratio	8.5	8.6	9.0	7.8	7.1

6.3.2.2 The Exwave semi

The wave impact phenomenon is not significantly dependent on the shape of the semi's columns – circular or square. The Exwave formula does not require any information of the shape. Therefore, the original motivation for studying the Exwave semi has more or less gone. Still, having modelled this vessel, simulations with SIMO have been carried out for this vessel. The result is shown in Table 6-6 which is directly comparable to the results for Deepsea Bergen in Table 6-5.

Table 6-6 Statistics for the Exwave semi-submersible. Three-hour simulations with sea states in Table 6-3

		$H_s = 5 \text{ m}$ $T_p = 7.1 \text{ s}$	$H_s = 6 \text{ m}$ $T_p = 8.1 \text{ s}$	$H_s = 7 \text{ m}$ $T_p = 9.1 \text{ s}$	$H_s = 8 \text{ m}$ $T_p = 10.1 \text{ s}$	$H_s = 9 \text{ m}$ $T_p = 11.2 \text{ s}$
Surge position (m)	Mean	0.00	0.00	0.00	0.00	0.00
	St. dev. WF	0.32	0.34	0.31	0.38	0.54
	St. dev. LF	1.27	1.73	3.16	3.68	3.06
	St. dev. tot.	1.32	1.78	3.20	3.73	3.16
	Minimum	-2.86	-3.47	-5.74	-7.20	-7.11
	Maximum	6.71	8.65	18.37	22.29	15.57
	Ratio	5.1	4.9	5.7	6	4.9
LF wave-drift force (kN)	Mean	418	551	809	922	881
	Standard dev.	431	561	816	914	870
	Minimum	0	0	0	0	0
	Maximum	3995	5364	8124	8349	6618
	Ratio	8.3	8.6	9.0	8.1	6.6

The comparison may have some interest, since the Exwave semi is a bigger vessel. Comparing the two tables, we see that the motion response of the Exwave semi in general is larger than that of the Deepsea Bergen. The difference in wave-drift loads reflects the difference in the corrected wave-drift coefficients (Figure 6-7).

6.3.2.3 Comparison of results from the two semi-submersibles

For the loads, the values of *Ratio* in Table 6-5 and Table 6-6 are about the same for the two semis, but the Exwave semi has somewhat larger *Ratio* values for the surge offset. This indicates, according to [16], that the motion response of Deepsea Bergen tends more towards gaussianity than the response of the Exwave semi. This further indicates that the damping ratio of Deepsea Bergen is lower (Although Table 6-2 states identical damping ratios for the two semis, these values are based on the mass-spring-damper analogy. The prescribed damping may therefore deviate from the true damping, which depends on how the filter and thruster delay affect the control system's characteristics). Most important for the difference in response is probably that Deepsea Bergen has tighter position control, owing to the larger controller bandwidth (see Table 6-2), which results in larger controller gains.

Also for the Exwave semi the response maximum is obtained for the second highest wave height. Rather than being a coincidence, this is caused by the fact that identical wave realizations are used for the two platforms.

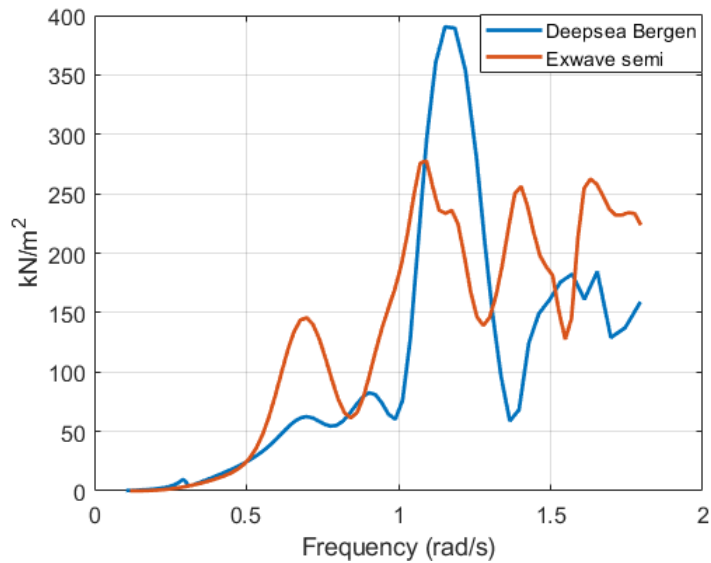


Figure 6-7 Corrected wave-drift coefficients for the two semis. Correction is carried for a significant wave height of 7 m

After the simulations had been carried out, it was discovered that the correction formula (14) had been applied slightly incorrectly for the Exwave semi, in that the number of columns had been set at six, rather than four. Since the other parameters in the formula, including the total water plane area, had been set correctly, the resulting error in the wave drift is comparatively small, as shown in Figure 6-8.

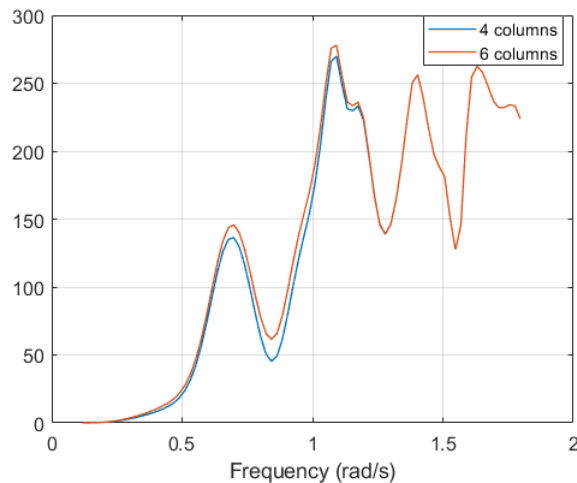


Figure 6-8 Corrected wave-drift coefficient for the Exwave semi assuming 4 (correct) columns and 6 (wrong) columns in the correction formula.

6.3.3 Probability of loss of position

The numbers labelled "Maximum" in Table 6-5 and Table 6-6 are sample maxima and as such estimates for the expected three-hour maxima. The probability of exceeding the expected maximum is in the order of 0.5. This means that by making observations in a number of three-hour intervals, the expected maximum will be exceeded in roughly half of them. For Rayleigh-distributed peaks, the probability of exceeding the expected

maximum is 0.53 (while the most probable maximum has an exceedance probability of 0.61). In the following, it is attempted to extract additional information about probability from the content in the two tables and the background simulations.

The statistical distribution of the response is complicated as it consists of the sum of LF and WF responses, which are distributed differently. The WF response, being approximately Gaussian and narrow-banded, have Rayleigh-distributed peaks. No known distribution formula exists for the LF response, but an approximate semi-empirical model for the LF maximum exists [16]. For the maximum of the combined (LF+WF) response, a rule of thumb is frequently used in want of a proper formula [9], [13]:

$$\hat{x}_{LF+WF} = \hat{x}_{LF} + 2\sigma_{WF} \quad (25)$$

Here, the circumflex accent stands for maximum, and σ denotes standard deviation (This expression applies when the LF response is predominant, in the opposite case an analogous expression applies).

To estimate the maximum in a time period of given length, a factor is frequently sought such that the maximum is expressed as

$$\hat{x} = C\sigma \quad (26)$$

where σ is the standard deviation of the process. The factor C depends on the type of the probability distribution, the sample size and what kind of maximum one wants, e.g. the expected maximum, the most probable maximum or a percentile. For a given percentile, q , the factor C becomes a function of q .

Assuming a given limit L_{LF} for the LF maximum \hat{x} , we seek the value of q that gives L_{LF} , i.e.

$$L_{LF} = C(q)\sigma_{LF} \quad (27)$$

The sought probability is solved from

$$q = C^{-1}(L_{LF}/\sigma_{LF}) \quad (28)$$

where C^{-1} denotes the inverse of the function C .

The expression for the function $C(q)$ is rather complicated. It is not shown here, but can be found in [13] and [16]. The parameters of the function $C(q)$ were found by running MIMOSA with a model of Deepsea Bergen and the wave states in Table 6-3.

For chosen limits of response,

$$L = \{7, 10, 15, 20\} \text{ m}$$

the corresponding LF limit was calculated as, (cf. (26)):

$$L_{LF} = L - \sigma_{WF} \quad (29)$$

The probability q was then calculated using (28). This was done for each limit, L , and each wave state. The result is shown in Table 6-7.

For the Exwave semi, the same factor $C(q)$, was used as for Deepsea Bergen. This was based on the assumption that basic type of distribution would be identical for the two vessels.

Table 6-7 Probability of exceeding given position limits. DSB = Deepsea Bergen, EXW = Exwave Semi

Pos. limit	Probability of exceedance									
	$H_s = 5$ m $T_p = 7.1$ s		$H_s = 6$ m $T_p = 8.1$ s		$H_s = 7$ m $T_p = 9.1$ s		$H_s = 8$ m $T_p = 10.1$ s		$H_s = 9$ m $T_p = 11.2$ s	
	DSB	EXW	DSB	EXW	DSB	EXW	DSB	EXW	DSB	EXW
7 m	0.511	0.349	0.621	0.810	0.966	0.9998	0.9992	0.99999	0.99991	0.99991
10 m	0.091	0.040	0.135	0.254	0.564	0.963	0.900	0.995	0.961	0.969
15 m	0.003	0.0008	0.006	0.016	0.077	0.492	0.298	0.738	0.430	0.492
20 m	0.0001	1.5E-5	0.0003	0.0009	0.008	0.130	0.053	0.291	0.093	0.124

Information like that shown in the table is useful as a criterion for when a given offshore operation can be carried out in a given wave state, which can be obtained from on-site wave measurements or a provider of metocean forecast. The table gives the probabilities of limit exceedance in a period of three hours. However, similar tables can be made for any duration.

The semi-empirical probability model behind the numbers in the table is complicated. The type of distribution of the LF response peaks depends on the damping in the system, cf. [16]. Like most approximate models, it has a range of validity. The results above are obtained for a DP-regulated vessel, which is strongly damped, and the model's applicability for such a damping level should be investigated. Further, the apparently crude way of combining LF and WF components of motion (25) could be subjected to study and hopefully improved.

As a point check of the results in Table 6-7, a 100-hour simulation was carried out with the model for Deepsea Bergen and the lowest wave state in the table. Figure 6-9 shows the cumulative distribution of the approximately 50 000 peaks. The sample maximum (encircled) is as high as 14.83 m, which is considerably larger than the second highest peak of 11.3 m. This indicates that the type of distribution is close to exponential, which according to the theory in [16] is the limit for strongly damped vessels. It is interesting to compare the occurrence of 14.83 m with the 3-hour exceedance probability for 15 m in Table 6-7. This value is 0.003 (for $H_s = 5$ m). Transformed to a 100-hour interval the 3-hour exceedance probability of 0.003 corresponds to an exceedance probability of 0.1. This means that we should expect a sample maximum of 15 m to occur in about one of ten 100-hour periods. This shows that the estimated probability of 0.003 of exceeding 15 m response in waves of $H_s = 5$ m and $T_p = 7.1$ s could be on the high side, but definitely not improbable.

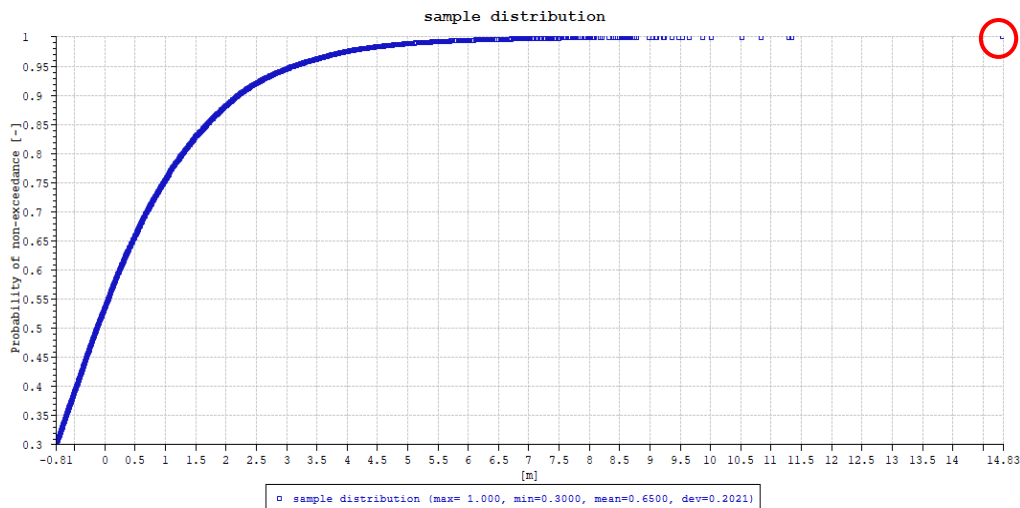


Figure 6-9 Cumulative distribution of peaks of surge motion from a simulation of 100 hours length with the model for Deepsea Bergen. The sample maximum is encircled.

6.3.4 Dependence of response on spectral peak period - probability curves

The choice of wave conditions for the study was based on the assumption that steep waves would create the largest force. Hence, to the selected five values of significant height, corresponding spectral peak periods were taken from the 1-year contour of statistical recurrence. To check the assumption, T_p was varied for each of the five values of H_s in Table 6-3. To get small statistical error, a duration of eighteen hours was simulated, and extremes of motion were estimated from Weibull distributions fitted to the data. The model for Deepsea Bergen was used.

The result is shown in the form of equiprobability curves in Figure 6-10 and on tabular form in Table 6-8.

Accepting the Weibull distributions as representative for the statistical response processes, the probability of any extremum of response can be calculated. The figure below shows an example. It is directly obtainable from Sima (the "workbench" of Simo). The probability level of 99.994 % in the figure is not comparable to the probabilities of 3-hour offset maxima in Table 6-7. Rather, it represents a point on the cumulative probability of the sample distribution of individual peaks in 18 hours. The parameter σ in the figure pertains to the fitted Weibull distribution. The lines represent values of offset peaks that have the same cumulative probability, which makes the peak periods comparable. The figure shows that for the smallest significant wave height ($H_s = 5$ m) the peak that corresponds to the 99.994 % probability is highest for the selected short period of 7.1 seconds (Table 6-3), but varies little with period from 8 seconds and upwards. For the other wave states, the lines have a negative slope. For the highest wave height ($H_s = 9$ m) the decline with period is most pronounced.

These results support the hypothesis behind the choice of the wave states, i.e. that short waves give larger motion response. Yet, longer periods may well give significant 3-hour maxima. If the criterion for operability is based on significant wave height only (and not also T_p), the probabilities for threshold exceedance in Table 6-7 must be calculated as a probability-weighted average over all relevant values of T_p .

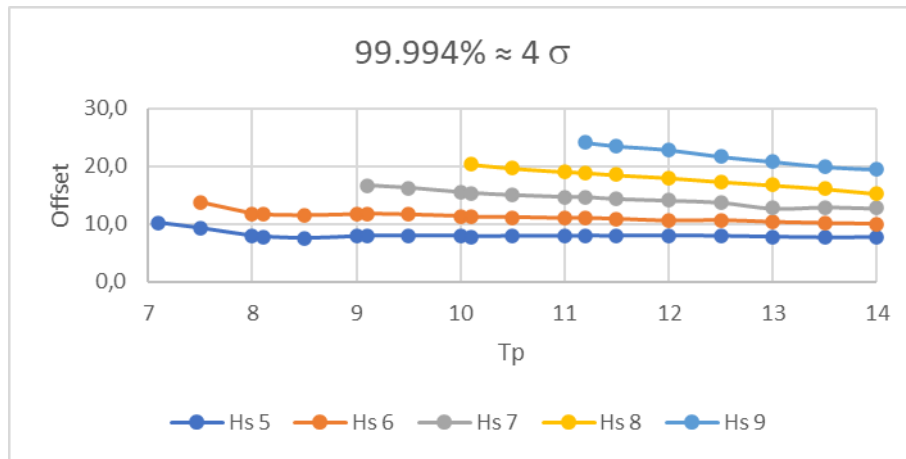


Figure 6-10 Lines of equal probability of surge peak offset as functions of spectrum peak period - one line for each significant wave height. The lines represent a probability of non-exceedance of 99.994 %

Table 6-8 Information of Figure 6-10 in tabular form

	Sigma 4																		
Hs/Tp	7,1	7,5	8	8,1	8,5	9	9,1	9,5	10	10,1	10,5	11	11,2	11,5	12	12,5	13	13,5	14
5	10,3	9,3	7,9	7,8	7,6	7,9	8,0	8,0	7,9	7,8	7,9	7,9	8,0	7,9	8,0	7,9	7,8	7,6	7,7
6		13,8	11,8	11,6	11,5	11,7	11,8	11,6	11,3	11,2	11,2	11,0	11,0	10,9	10,5	10,6	10,3	10,1	10,0
7							16,6	16,2	15,5	15,4	15,0	14,7	14,7	14,4	14,1	13,7	12,7	12,9	12,7
8										20,4	19,7	19,1	18,9	18,5	18,0	17,3	16,7	16,1	15,2
9													24,1	23,5	22,8	21,6	20,8	19,9	19,4

To give an indication of the agreement between the results in Table 6-8 and Table 6-7 a rough comparison is made: The offset value of 10.3 m for $H_s = 5$ m and $T_p = 7.1$ s in Table 6-8 has a probability of non-exceedance of 0.99994 by choice. Assuming the mean period of oscillation to be 7.1 s, the number of peaks become 1521. Assuming independently distributed peak heights (which is questionable), the probability of exceeding 10.3 m should then be $P(x > 10.3) = 1 - 0.99994^{1521} = 0.087$. This compares well with the probability 0.091 of exceeding 10 m in Table 6-7 (Deepsea Bergen).

6.3.5 Further analysis of results

For the base case in Table 6-5 ($H_s = 7$ m, $T_p = 9.1$ s) the wave-drift force and the surge response for Deepsea Bergen are shown in Figure 6-11. The tallest force peak and corresponding response peak happen just before 1780 seconds. The magnitude of the peaks corresponds to the maximum values for 7 m wave height in the table (4377 kN and 11.44 m, respectively).

Figure 6-12 shows a close-up on the circumstances around the extreme event. The wave-drift force has the appearance of a sequence of peaks of short duration, i.e. less than twenty seconds. According to paragraph 5.2.3.2 and Figure 5-12, a pulse of this duration may cause a response that is not much less than a response created by an ideal impulse. The response shown in Figure 6-12 is the total of LF and WF response, the WF components appearing as ripple on top of the LF response. It is seen that the response more or less follows the smoothed wave-drift load, yet with a lag of fourteen seconds. The lag is expected, considering the delays in the wave + noise filter and thruster response.

For the base case, the spectra of wave-drift force and surge motion are shown in Figure 6-13 and Figure 6-14. The force has considerable power from zero and up to the peak frequencies of the wave spectra (0.09 -0.14 Hz). This is useful information for an evaluation of the simplified model described in Chapter 5.

The response spectra - shown with identical scaling – are damped out by the mass of the vessel and the DP system and have negligible power above 1/100 Hz (For the largest sea state, some WF power is barely discernible around 0.09 Hz)

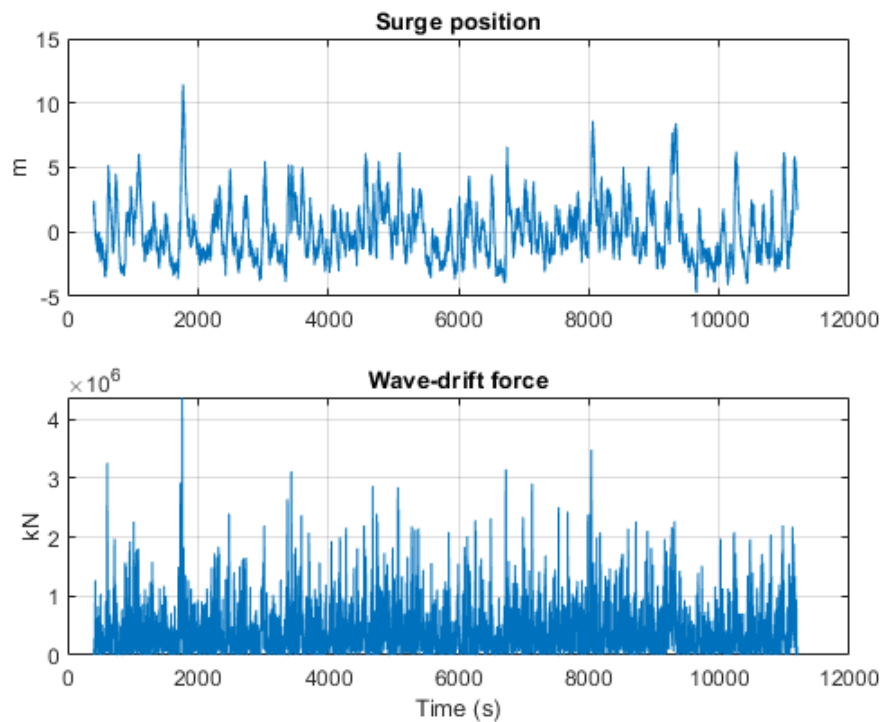


Figure 6-11 Deepsea Bergen surge response and wave drift load ($H_s = 7$ m, $T_p = 9.1$ s)

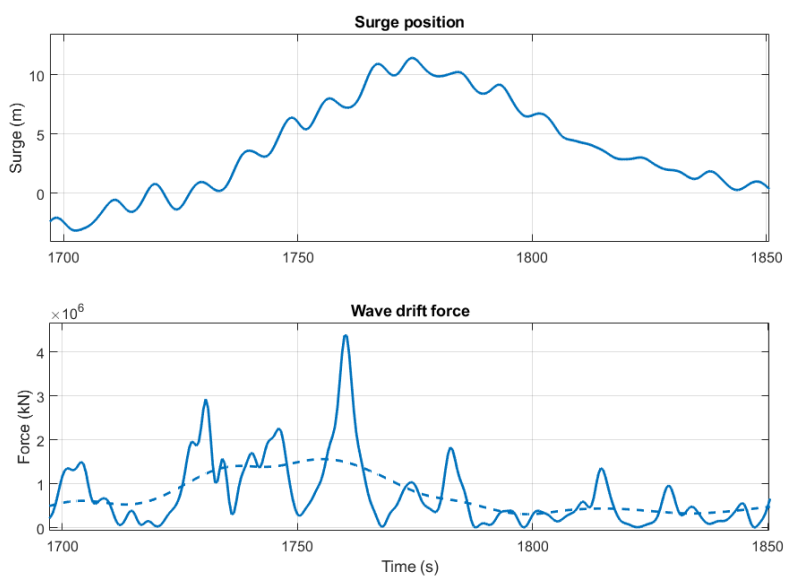


Figure 6-12 Deepsea Bergen surge response and wave-drift load around tallest peak ($H_s = 7$ m, $T_p = 9.1$ s). Dashed line is smoothed force.

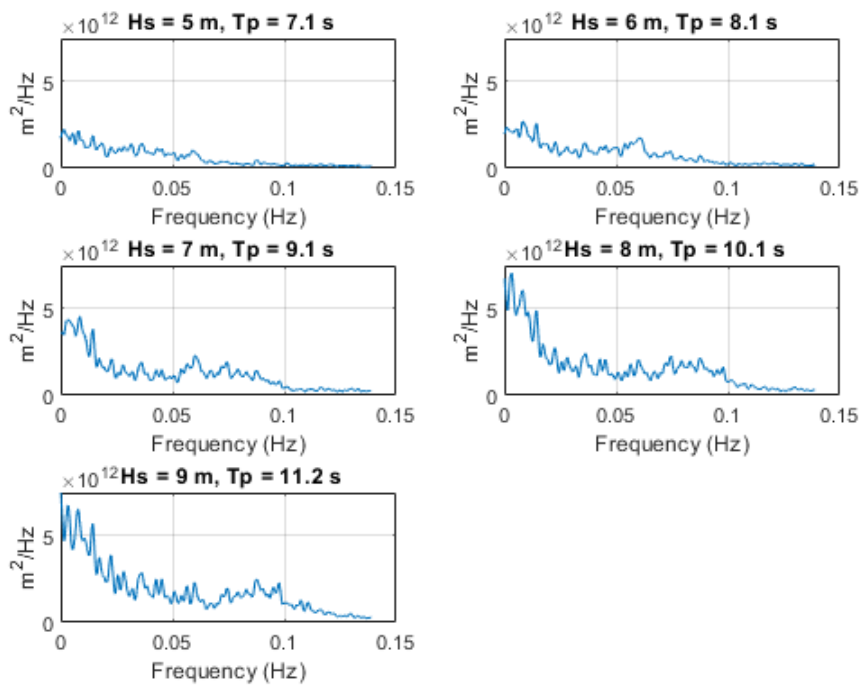


Figure 6-13 Spectra of wave drift force in surge for the five sea states (Deep Sea Bergen)

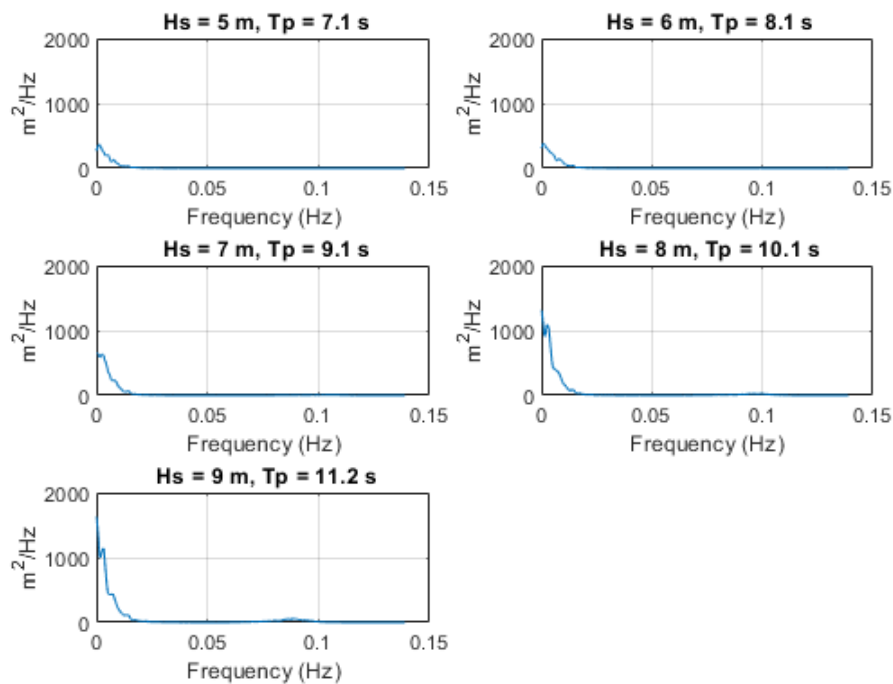


Figure 6-14 Spectra of surge response for the five sea states

7 THE INFLUENCE OF THE DP SYSTEM ON THE RESPONSE

In the study, the characteristics of the DP system has remained more or less constant. The backbone of the DP controller is the proportional feedback, which has been chosen such that the undamped natural period becomes about 100 seconds. For Deepsea Bergen this resulted in a gain of about 120 kN/m. For the Exwave semi the gain was about 200 kN/m. The derivative gain or damping was set to give a damping ratio of about 0.7 based on the mass-spring-damper analogy.

In general, higher controller gains will reduce the position error. As described in Chapter 5, the control action is delayed by the thruster dynamics and the wave + noise filter. For a slow disturbance this delay matters little. For an abrupt disturbance, however, the position error will evolve with little restraint from the thrusters. This is of course, exactly what is the purpose of the wave filter, but as demonstrated in paragraph 5.2.3.2, a pulse of 20 seconds duration – well above the normal range wave periods - will also evade control.

Comment: A wave filter can be designed with any frequency-discriminating sharpness, but high sharpness will create a phase lag that is inadmissible in a feedback system

As concluded in the foregoing, the likely reason for loss of position in moderate wave conditions is a group of high and steep waves. The passing of such a group may last less than a minute.

There are a number of ways the resulting vessel responses can be reduced, e.g.:

Increase the controller gains.

Higher gains will in general give smaller response. However, increasing the gains above a certain limit will make the control system unstable.

Reduce strength of wave + noise filter

The filter reduces the amount of WF motion and measurement noise that is fed to the thrusters. By removing the filters (some noise filtering must be retained), the action of the DP controller will become more prompt. However, the thrusters will become noisier, more exposed to wear and demand more fuel. So, DP controller design is a tradeoff between these deficiencies and effective motion regulation.

Alternative instrumentation

The main measurement today is position measurement with satellite and inertial navigation devices. The vessel velocity, which is needed by the controller, is not readily measured. Acceleration is cheap to measure, and can be processed to give velocity. However, there will still be a need for strong lowpass or band-stop filtering, which will cause delays. Moreover, a horizontal accelerometer will be strongly affected by the vessel's rolling and pitching motion and requires correction from devices for measurement of angular motion. Such correction is done in most so-called *motion reference units* (MRU's) today. Still, there is a lower frequency limit for the usefulness of an MRU.

8 SUGGESTIONS FOR FURTHER WORK

The work carried out in this study has been mainly phenomenological, in that a certain hypothesis has been tested with simplified models and a limited amount of calculation and simulation with a comprehensive state-of-the art model like model Simo. Only one component of vessel motion (surge) has been considered.

To complete the picture, the following tasks are suggested:

- Study the responses of other relevant vessel modes, i.e. sway, roll, pitch and yaw.
- Study composite responses, e.g. the motions of a gangway, which may have a complex pattern of motion that will include the resonant motion of rolling and pitching.
- Develop better probabilistic models for vessel response, e.g. how to combine WF and LF response and how to produce more reliable estimates of limit exceedance.
- Establish criteria for safe vessel operation based on metocean statistics
- Investigate the possibilities and limits of the DP system, as discussed in Chapter 7, to recommend DP settings under varying metocean conditions, and possibly suggest new ways of instrumenting.

9 ACKNOWLEDGEMENT

SINTEF Ocean thanks Odfjell Drilling for permission to use the numerical model for Deepsea Bergen in the study.

10 CONCLUSION

There have been a number of cases where the position limits for DP-regulated semisubmersibles have been exceeded in sea states that can be classified as normal operating conditions. One hypothesis for these events is that the semis had been driven past their limits by a slamming load from a single high and steep wave. Other possible causes for the loss of position could be viscous loading on the semis' columns or the accumulated effect of a group of tall waves.

The slamming hypothesis was tested by assuming an extreme slamming event in a sea state of 7 m significant height and a spectral peak period of 9.1 s. The wave was given the amplitude of 6.7 m, which corresponds

to the most probable maximum in a period of three hours. Assuming the wave to form a vertical front of a height equal to its amplitude at the time it hit the columns and setting the velocity equal to the celerity corresponding to the spectrum peak period, the slamming load and its duration were calculated.

The behaviour of a vessel under DP control resembles that of a mass-spring-damper system, however, with one exception: The restoring force is not immediate as by a spring but delayed as a result of filtering in the DP controller before created by the thrusters. Assuming a typical DP system and a semi similar to Deepsea Bergen, the above slamming event resulted in a maximum excursion of 2.4 m, which is twice as much as the excursion obtained with a mass-spring-damper model of similar mechanical characteristics. Still, a slamming load is not considered to be a single source of loss of position.

The vessel + DP system model used in the calculation was made as a linear model with one degree of freedom of motion. The model is a combination of: 1) a mass-spring-damper model resembling the mechanical properties of Deepsea Bergen, 2) a Kalman-Bucy state observer 3) a proportional + derivative controller, and 4) a 1st-order dynamic model with a time constant of 10 seconds to represent the thruster response.

The model was used to investigate essential behaviour of the DP system. Although the thruster dynamics will cause delay in the thruster action, it was found that the main reason for the bigger maximum excursion as compared to the mass-spring-damper system, was the delay in the state observer (which incorporates the wave + noise filter). In particular, the problem can be tracked down to the delay in the velocity estimate: To restrain the excursion caused by an abrupt disturbance, quick velocity feedback is required

Viscous force on the columns of a semisubmersible vessel is not included in models based on potential theory. Drag force on the columns of Deepsea Bergen was calculated for the same wave state as in the slamming analysis. Although quadratic in velocity, the viscous drag will generate an additional force that is strongly correlated with the oscillatory potential force from the waves. The magnitude of this force is found not to be a cause of excessive vessel motion.

In the Exwave joint industry project an approximate formula for increased wave-drift loading has been developed. The formula applies to semi-submersible vessels and includes the extra slow-drift loads on the columns due to non-linear effects, in particular viscous force. In addition, the formula includes a modification to the drift force when current is present. To study the effect of the "Exwave formula" simulations with Simo were carried out with two numerical models. One model was Deepsea Bergen, for the occasion fitted with thrusters and DP. The other model represents an anonymous semi-submersible. This model is referred to as the *Exwave semi*. It has columns of square cross-section in contrast to the Deepsea Bergen, which has circular columns. However, the cross-sectional shape of the columns is of minor importance and is not used by the Exwave formula.

Five wave states with H_S from 5 m to 9 m to represent possible operation conditions were chosen for the simulations. For each H_S the smallest spectral peak period occurring on the 1-year probability contour was chosen. Thus, each (H_S, T_p) pair has a mean return time of one year.

From the simulations with Simo and presenting the response as graphs of cumulative distribution of peaks, it was demonstrated that, for a given H_S of 7 m, the wave-drift force corresponding to the chosen short spectral peak period of 9.1 s is significantly larger than the force obtained for a period of 13 s, which is typical for that H_S . Further, adding swell to the wave causes insignificant increase in the wave-drift force. For the same wave state, it was also demonstrated that applying the Exwave formula gives a considerable increase in the force.

It is characteristic of wave drift loads that the maximal load is much larger than the mean force or the standard deviation as compared to linear processes. For the five chosen wave states, the 3-hour maximal responses range from 7 m to 13 m (Deepsea Bergen). For the wave state with $H_S = 7$ m and $T_P = 9.1$ s, Simo gives a response maximum of 11.4 m. The wave-drift force in this case consists of a number of pulses of less than 20 seconds duration. These pulses are not effectively counteracted by the DP system.

The maximum of 11.4 m is much larger than the excursion of 2.4 m caused by the rare slamming event. From this, the conclusion must be that if an excessive excursion happens to a DP-controlled semisubmersible, the most probable cause will be a wave group that creates large wave-drift force.

Simulations with the model for the Exwave semi and the five wave states gives responses that on the whole are larger than those obtained with Deepsea Bergen. The Exwave semi is a bigger vessel and not moved so easily as Deepsea Bergen, but this is more than outweighed by the larger wave-drift forces. For the Exwave semi the second largest significant wave height (8 m) caused a larger response than the wave of 9 m significant height. The reason for this is the smaller wave period for the wave of 8 m, as shorter waves in general will produce larger wave-drift force.

From the simulated results, the probability of exceeding offset limits of 7, 10, 15 and 20 metres were estimated for the two semis. The estimation is complicated, since the response is a combination of LF and WF components, which have statistical distributions of very different character. The WF peaks of motion can be modelled by the well-known Rayleigh distribution. For the peaks of LF motion an approximate semi-empirical distribution model exists. For the combination of LF and WF peaks a common rule of thumb was used. Although based on approximate and uncertain models, point checks using Weibull distributions fitted to long simulation runs shows good agreement with the estimated probabilities of limit-exceedance.

The probabilities of limit exceedance were calculated for the five wave states on the 1-year contour. To find the 1-year (say) probability of limit exceedance for a given wave height, regardless of period, the calculation of probability must be carried out as a weighted sum of for all periods within the 1-year contour.

Throughout the study, a DP system with a bandwidth of about 1/100 Hz has been used. Tighter control (stronger feedback) will give smaller motion response, but too large gains will cause instability. To improve the DP system's response to sudden disturbances, weaker WF and noise filtering can be used. However, this will let more WF and noise through to the thrusters.

Some suggestions for topics of further work are given

11 REFERENCES

- [1] Petroleumstilsynet, "Gransking av utilsiktet frakopling av gangbro på Floatel Endurance 29.2.2020". Granskingsrapport. 18.6.2020
- [2] Kongsberg, "Investigation report Floatel Endurance Emergency Lift 29 Feb 2020", Project Dp6705711, 2020-03-08
- [3] Myrhaug, Dag, "Uregelmessig sjø", Kompendium SIN1015 Marin dynamikk, Faculty of engineering Science and Technology – NTNU Trondheim Norwegian University of Science and Technology, 2002
- [4] Wienke, J. and Oumeraci, H., "Breaking wave impact force on a vertical and inclined slender pile – theoretical and large-scale model investigations", Coastal Engineering 52 (2005) 435-462, Elsevier, Science direct, 2005
- [5] Morison, J. R., O'Brian, M. P., Johnson, J. W., Schaaf, S. A., "The force exerted by surface waves on piles", Petroleum Trans. 189, 149-157, 1950



- [6] Faltinsen, O. M., "Sea Loads on Ships and Offshore Structures", Cambridge University Press, 1990.
- [7] Sarpkaya, T., "Force on a circular cylinder in viscous oscillatory flow at low Keulegan-Carpenter numbers", Cambridge University Press, 1986, Calhoun: The NPS Institutional Archive DSpace Repository
- [8] Fonseca, N., Ommani, B., Stansberg, C. T., Bøckmann, A., Birknes-Berg, J., Nestegård, A., de Hauteclocque, G., Baarholm, R., "Wave Forces and Low Frequency Drift Motions in Extreme Seas: Benchmark Studies", Paper OTC-27803-MS, Offshore Technology Conference, Houston, USA, 2017
- [9] DNV GL, "Position mooring", Offshore standards, DNVGL-OS-E301, July 2018
- [10] Kaasen K. E., "Time domain model representation of standard wind gust spectra", Paper No. 99-ISC-281, ISOPE, 1999
- [11] Balchen, J. G., Fjeld, M., Solheim O. A., "Reguleringsteknikk, Bind 3, Multivariable systemer", Tapir forlag 1970. (In Norwegian)
- [12] SIMO 4.18.2 User Guide SINTEF Ocean, December 10, 2020
- [13] MIMOSA User's Documentation, Program version 6.3-10, SINTEF Ocean, 2019-10-01
- [14] Reistad, M., Breivik, Ø., Haakenstad, H., Aarnes, O. J., Furevik, B. R., Bidlot, J.-R., "A high-resolution hindcast of wind and waves for the North Sea, the Norwegian Sea, and the Barents Sea", Journal of geophysical research. Oceans. Vol. 116, Issue C5, May 2011
- [15] DNV GL and SINTEF Ocean, "Handbook on low-frequency wave forces and response – guidelines and recommendations", Report No. 2017-0251, Rev.2 Document No. 1LPCNZ2-13, 2017-09-13
- [16] Stansberg, C. T., "Prediction of Extreme Slow-Drift Amplitudes", Paper No. 00-6135 Proc. 19th OMAE Conference (ASME), New Orleans, LA, USA, 2000